Theses and Dissertations   Student Graduate Works

3-9-2009

Low Probability of Intercept Waveforms via Intersymbol Dither Performance under Multipath Conditions

Jonathan K. Keen

Follow this and additional works at: https://scholar.afit.edu/etd

Part of the Digital Communications and Networking Commons, and the Information Security Commons

Recommended Citation

LOW PROBABILITY OF INTERCEPT WAVEFORMS
VIA INTERSYMBOL DITHER
PERFORMANCE UNDER MULTIPATH CONDITIONS

THESIS

Jonathan Kingston Keen, Captain, USAF

AFIT/GE/ENG/09-23

DEPARTMENT OF THE AIR FORCE
AIR UNIVERSITY

AIR FORCE INSTITUTE OF TECHNOLOGY

Wright-Patterson Air Force Base, Ohio

The views expressed in this thesis are those of the author and do not reflect the official policy or position of the United States Air Force, Department of Defense, or the United States Government.

AFIT/GE/ENG/09-23

Low Probability of Intercept Waveforms via Intersymbol Dither Performance Under Multipath Conditions

THESIS

Presented to the Faculty

Department of Electrical and Computer Engineering

Graduate School of Engineering and Management

Air Force Institute of Technology

Air University

Air Education and Training Command

In Partial Fulfillment of the Requirements for the

Degree of Master of Science in Electrical Engineering

Jonathan Kingston Keen, B.S.E.E.

Captain, USAF

March 2009

AFIT/GE/ENG/09-23

Low Probability of Intercept Waveforms via Intersymbol Dither Performance Under Multipath Conditions

Jonathan Kingston Keen, B.S.E.E.

Captain, USAF

Approved:

/signed/		5 Mar 2009
Dr. Richard K. Martin (Chairman)		date
/signed/		5 Mar 2009
Dr. Michael A. Temple (Member)		date
/signed/		5 Mar 2009
Dr. Matthew C. Fickus (Member)		date

AFIT/GE/ENG/09-23

Abstract

This thesis examines the effects of multipath interference on Low Probability of Intercept (LPI) waveforms generated using intersymbol dither. LPI waveforms are designed to be difficult for non-cooperative receivers to detect and manipulate, and have many uses in secure communications applications. In prior research, such a waveform was designed using a dither algorithm to vary the time between the transmission of data symbols in a communication system. This work showed that such a method can be used to frustrate attempts to use non-cooperative receiver algorithms to recover the data. This thesis expands on prior work by examining the effects of multipath interference on cooperative and non-cooperative receiver performance to assess the above method's effectiveness using a more realistic model of the physical transmission channel.

Both two and four ray multipath interference channel models were randomly generated using typical multipath power profiles found in existing literature. Different combinations of maximum allowable symbol delay, pulse shapes and multipath channels were used to examine the bit error rate performance of 1) a Minimum Mean Squared Error (MMSE) cooperative equalizer structure with prior knowledge of the dither pattern and 2) a Constant Modulus Algorithm (CMA) non-cooperative equalizer. Cooperative MMSE equalization resulted in approximately 6-8 dB BER performance improvement in E_b/N_o over non-cooperative equalization, and for a full range symbol timing dither non-cooperative equalization yields a theoretical BER limit of $P_b=10^{-1}$. For 50 randomly generated multipath channels, six of the four ray channels and 15 of the two ray channels exhibited extremely poor equalization results, indicating a level of algorithm sensitivity to multipath conditions.

Acknowledgements

I would like to thank my Advisor, Dr. Richard Martin for his continued guidance and neverending store of patience throughout the thesis process. I couldn't have asked for a more supporting mentor.

I also owe a great deal to classmates from the Communications lab. Anytime I needed encouragement or a sounding board for my latest idea, they were there. They'll never know how important that support was to me during my tenure at AFIT.

Most importantly, I would like to thank my wife for her constant patience and support. I couldn't have done this without her.

Jonathan Kingston Keen

Table of Contents

List of Figures

List of Tables

List of Symbols

List of Abbreviations

xiv

Low Probability of Intercept Waveforms
via Intersymbol Dither
Performance Under Multipath Conditions

I. Introduction

1.1 Motivation

As the role of technology grows on the battlefield, the ability to sustain secure communications links has become vital to military operations [9]. With this need for secure communications over a broad range of activities and environments, wireless communications systems have become increasingly popular for military use [15]. The flexibility provided by wireless broadcasting systems transmitting over large areas also makes them vulnerable to detection and eavesdropping by third parties. As such, a great deal of current communications research focuses on ways to mitigate the risk of eavesdropping, detection, and exploitation of wireless communication systems.

Three basic areas of research into reducing the vulnerability of friendly transmissions to eavesdropping and exploitation are Low Probability of Detection (LPD), Low Probability of Interception (LPI), and Low Probability of Exploitation (LPE). LPD and LPI deal with methods to prevent or make it difficult for a non-cooperative receiver to be able to pick out the transmitted signal of interest from environmental noise or other signals [14]. For example, spread spectrum and frequency hopping are LPI/LPD methods in that they make the transmitted signal difficult to detect or intercept [17]. LPE methods focus on preventing any meaningful extraction of data from the transmitted signal of interest by non-cooperative receivers and third parties.

Multipath interference is a common issue in wireless communication systems, and is caused by a transmitted signal reaching the receiver by one or more time delayed paths by reflecting off of objects in the transmission environment [14]. These

1

delayed transmission paths can then interfere with the desired transmitted signal, causing a degradation in system performance. This thesis examines the effects of multipath interference on the intentional Intersymbol Interference (ISI) waveform designed in [8] to prevent non-cooperative receivers from determining the transmitted communications symbols.

1.2 Problem Statement

Because of the proliferation and widespread use of wireless communications for military and civilian use, communications have become vulnerable to eavesdropping, interception, and exploitation by unintended recipients. As such, strategies intended to reduce these risks associated with wireless broadcast transmissions such as LPI, LPD, and LPE techniques are desirable. One strategy is to utilize techniques designed to make it difficult for non-cooperative receiver designs to detect or intercept the communications waveform. Previous research by [8] developed a waveform designed to perform this task, and validated its effectiveness over a Line of Sight (LOS) channel.

This thesis will develop several different multipath models, validate them, and test the performance of the ISI waveform developed in [8] under multipath conditions. The ISI waveform modifies Differential Phase Shift Keyed (DPSK) modulation to frustrate non cooperative receiver strategies. This is accomplished by inserting ISI into the transmitted waveform to disrupt accurate non cooperative symbol estimation [8]. The ISI waveform achieved symbol estimation accuracy close to optimal DPSK performance over a LOS channel at the cost of additional receiver complexity to mitigate the ISI. Any additional complexity incurred by the addition of multipath interference is examined, as well as the potential performance loss of a non-cooperative receiver compared to a cooperative receiver designed to account for ISI and multipath.

1.3 Thesis Organization

Chapter 2 reviews the pertinent background information to the problem, and provides any necessary conceptual derivations. Topics covered include multipath

2

Interference, the design of the ISI waveform, and the communications model used throughout the thesis. Chapter 3 details the development of the models and simulations, and provides validation of these models. This includes the selection of the multipath models, and the development and design of a cooperative receiver model to equalize the ISI and multipath. Chapter 4 presents the simulation results, detailing the performance of the waveform under multipath conditions. Comparisons to analytical results and previous research are also presented. Chapter 5 presents the conclusions drawn from simulations in Chapter 4, and provides recommendations for future research in the problem area.

3

II. Background and Literature Review

2.1 Overview

This section begins by providing an overview of some common strategies for securing wireless communications. The remainder of the chapter covers background related to the modeling of ISI in wireless communications. A review of types of multipath models is presented, along with the different aspects of multipath. Two basic classes of equalizers are presented; cooperative and non-cooperative, or blind equalizers. Cooperative equalizers make use of some *apriori*, or prior, knowledge of the transmitted signal of interest in order to equalize ISI and other degrading effects, while blind equalizers attempt to equalize these same effects with minimal or no prior knowledge of the transmitted signal. An overview of the intentional ISI waveform using symbol dither developed in [8] is also provided.

2.2 Existing Secure Communications Strategies

Encryption is one of the most widely used methods of securing communications, and is used in applications such as computer networking, secure mobile phones, etc. The main goal of encryption is to prevent an unauthorized user from extracting meaningful information from the transmitted signal, protecting the transmitted data contained within. Encryption techniques typically use an encryption/decryption key that is provided to the intended users, and without this decryption key a cooperative receiver will not be able to extract the data from a transmitted signal. The security of this method is derived from the inability of an unauthorized party to obtain the key, even if they have some knowledge of the encryption and transmission methods used [17].

Frequency hopping involves changing the carrier frequency of the modulated signal, typically according to a pseudorandom sequence. A cooperative receiver uses knowledge of this pseudorandom sequence to know when to switch receive frequencies to locate and demodulate the signal. Two types of frequency hopping systems are slow and fast hopping systems. Slow hopping systems remain at a particular carrier

frequency for a block of transmitted symbols, while a fast hopping system changes carrier frequencies after every symbol. Without access to the pseudorandom sequence driving the carrier frequency changes, a non-cooperative receiver is forced to locate the new carrier after each hop before attempting demodulation. As such, a frequency hopping system must switch carriers quickly enough to prevent a non-cooperative receiver from being able to detect the change and match frequencies [17].

Spread spectrum techniques provide security by making it difficult for an unintended user to detect the signal at all. Spread spectrum methods smear the modulated signal over a very large bandwidth by mixing it with a pseudorandom code. As this disperses the signal power across this large bandwidth, it becomes much less likely that a third party receiver would be able to detect the transmitted signal within the noise of the transmission environment [17]. As in frequency hopping systems, a cooperative receiver must have knowledge of the pseudorandom mixing code to despread the transmitted waveform and reconstruct the original transmitted signal for demodulation. As a non-cooperative receiver is unlikely to have access to the code used for spreading the transmitted signal it is less likely to be able to extract any useful information, providing an additional layer of communication security [1].

2.3   ISI and Equalization

Digital communications systems transmit information as a series of communications symbols representing binary data. In a very basic signalling scheme, these communications symbols are transmitted back to back, with the end of one transmitted symbol marking the beginning of the next. As all practical pulse shapes used for transmission of symbols are bandlimited, there is a limit to the speed at which the communications system can alter the transmitted waveform. This can cause the symbols to mix or blur together, creating ISI [5]. Also, as these symbols are transmitted through some kind of physical media, e.g. through the air in the case of wireless transmissions, the received signal is an attenuated and distorted version of the original transmitted symbol. These effects are worsened in wireless communications as each

5
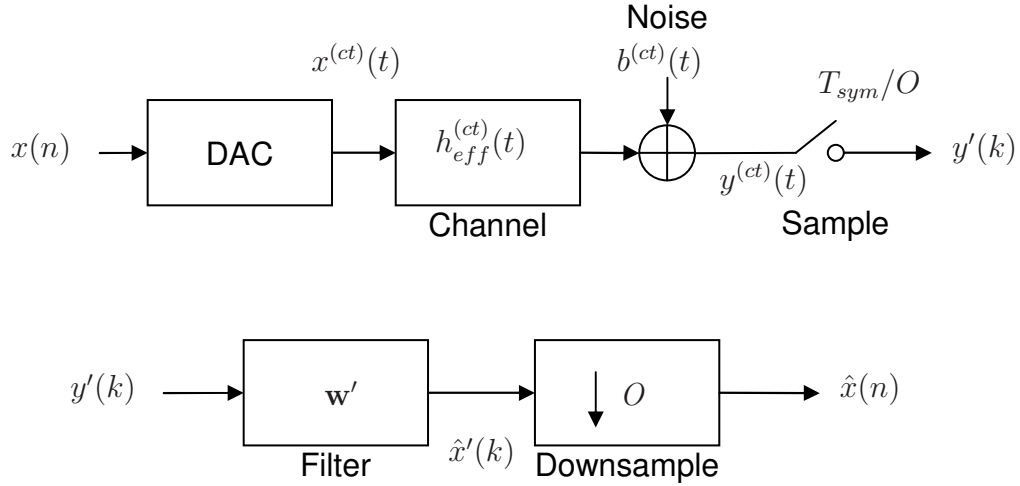
Figure 2.1: Baseband communications model [8]

transmitted symbol can take multiple paths to the receiver with each path causing independent amplitude and phase distortions on the signal. This is known as multipath, and an overview of its effects is provided in Section 2.5 along with possible modelling methods.

These distortions can be modeled as a linear time-invariant system according to (2.1), which maps the transmitted signal $x(t)$ to received signal $y(t)$ using impulse response $h(t)$ [14].

$$y(t) = \int_{-\infty}^{\infty} x(\lambda) h(t - \lambda) \, d\lambda \tag{2.1}$$

This section examines the baseband communications model presented in Figure 2.1. The transmitted symbol sequence is a series of discrete symbols denoted by $x(n)$. The digital to analog converter (DAC) block converts the discrete series $x(n)$ to a *continuous time* (*ct*) waveform with symbol impulses occurring every T_{sym} seconds. The transmitted signal is then acted on by the effective channel impulse response $h_{eff}^{(ct)}(t)$ which contains the pulse shape $f^{(ct)}(t)$, the physical channel impulse response $h_{phys}^{(ct)}(t)$, and a matched filter in the receiver $f^{(ct)}(-t)$, described in (2.2). The received signal $y^{(ct)}(t)$ is then sampled by an oversampling factor of O times per T_{sym} [8].

Equation (2.2) shows the form of $h_{eff}^{(ct)}(t)$. It is important to note that $h_{phys}^{(ct)}(t)$ can also contain multipath effects characterizing the different paths the signal can take to the receiver. Also note that the pulse shapes used in this thesis are both real and symmetric, so that the pulse shape and the matched filter are identical to one another.

$$h_{eff}^{(ct)}(t) = f^{(ct)}(t) \star h_{phys}^{(ct)}(t) \star f^{(ct)}(-t) , \tag{2.2}$$

where

$$f^{(ct)}(t) = \text{Pulse shape (and matched filter) ,}$$
$$h_{phys}^{(ct)}(t) = \text{Physical channel impulse response.}$$

In the communications model presented in Figure 2.1, the N transmitted symbols are represented by a series of discrete terms, $x(n)$. The signal after matched filtering at the receiver can be written as

$$y^{(ct)}(t) = \sum_{n=0}^{N-1} x(n) h_{eff}^{(ct)}(t - nT_{sym} - t_o) + b^{(ct)}(t), \tag{2.3}$$

where $h_{eff}^{(ct)}$ is the effective channel impulse response, t_o is the sampling synchronization offset, and $b^{(ct)}(t)$ is an additive noise signal.

The additive noise signal $b^{(ct)}(t)$ is the environmental noise through the transmission channel that has passed through the matched filter. All noise used in this thesis is assumed to be Additive White Gaussian Noise (AWGN), denoted as $\nu^{(ct)}(t)$. The resulting noise signal is shown in (2.4).

$$b^{(ct)}(t) = \int_{-\infty}^{\infty} f^{(ct)}(\tau) \upsilon^{(ct)}(t - \tau) d\tau \tag{2.4}$$

7

Due to the oversampling factor O, (2.3) can be rewritten as (2.5) with t replaced by kT_{sym}/O to represent the higher sampling rate of T_{sym}/O samples per second. With this substitution, the received signal after matched filtering is expressed as

$$y^{(ct)}\left(\frac{kT_{sym}}{O}\right) = \sum_{n=0}^{N-1} x(n)h_{eff}^{(ct)}\left(\frac{kT_{sym}}{O} - nT_{sym} - t_o\right) + b^{(ct)}\left(\frac{kT_{sym}}{O}\right) . \qquad (2.5)$$

The discrete analog of $y^{(ct)}\left(\frac{kT_{sym}}{O}\right)$ is given in (2.6) and represents the oversampled discrete received sequence before equalization.

$$y'(k) = y^{(ct)}\left(\frac{kT_{sym}}{O}\right) \qquad (2.6)$$

Equalization attempts to minimize or remove the effects of ISI and other channel effects via post processing within the communications receiver. This can be done using many different algorithms and techniques. One common technique used for equalization is filtering. Filtering attempts to modify the received signal in some way that makes the communications symbols distinct, effectively cancelling out or inverting the effect of the channel [14]. The digital transverse filter is a linear-time invariant system defined by the discrete impulse response w' which acts on the discrete received symbols $y'(k)$ to produce a time delayed estimate of the transmitted symbols, defined as $\hat{x}'(k)$ [11]. The digital transverse filters' operation can be described using the discrete convolution sum,

$$x'(k) = w'(k) \star y'(k) = \sum_{m=0}^{M-1} w'(m)y'(k - m) . \qquad (2.7)$$

Here, $\hat{x}'(k)$ is the oversampled discrete estimated input sequence after equalization, and is then downsampled by the oversampling factor O to produce the estimated output sequence $\hat{x}(n)$. Note that $\hat{x}(n)$ is approximately equal to $x(n - \delta)$, and δ is

8

some fixed delay that maps the nth estimated symbol to the nth minus δ transmitted symbol.

The mathematical model for the filtering operation given in (2.7) is only valid if the channel response is static, and in most real physical systems the channel impulse response varies as a function of time [14]. For a non time varying channel, a preset equalization method is sufficient to equalize the channel. In a preset equalization method, the equalization taps needed to invert the static channel are calculated and then applied to each received signal, with no need to adjust the filter taps. However, for time varying channels, some method of adjusting the filter taps over time to account for changing channel conditions is needed. An adaptive equalizer is one that has the ability to update the filter taps either continuously or at set periodic times. The convergence rate is the key parameter of an adaptive filter method in regards to its ability to equalize a time varying channel. The convergence rate is a measure of how quickly the adaptive method can change the filter taps, and if the channel variation exceeds the convergence rate of the adaptive filter, symbol estimation performance is degraded [14].

A subset of non-cooperative receivers using blind adaptive equalization techniques are examined in this thesis. These techniques are designed to mitigate the channel effects with little or no knowledge of the channel by utilizing the statistics of the source signal [5]. These types of blind equalization techniques are ideal for use in the design of a non-cooperative receiver developed for eavesdropping, and the dither algorithm detailed in Section 2.6 varies the channel impulse response beyond the convergence rate of these blind techniques to prevent meaningful third party demodulation of the transmitted signal.

2.3.1 Convolution Matrix Model. The discrete linear convolution process described in Section 2.3 can also be expressed in matrix form. As convolution is a computationally expensive calculation, recasting the convolution process as a series of matrix operations allows for faster and more efficient computation. It is important to

9
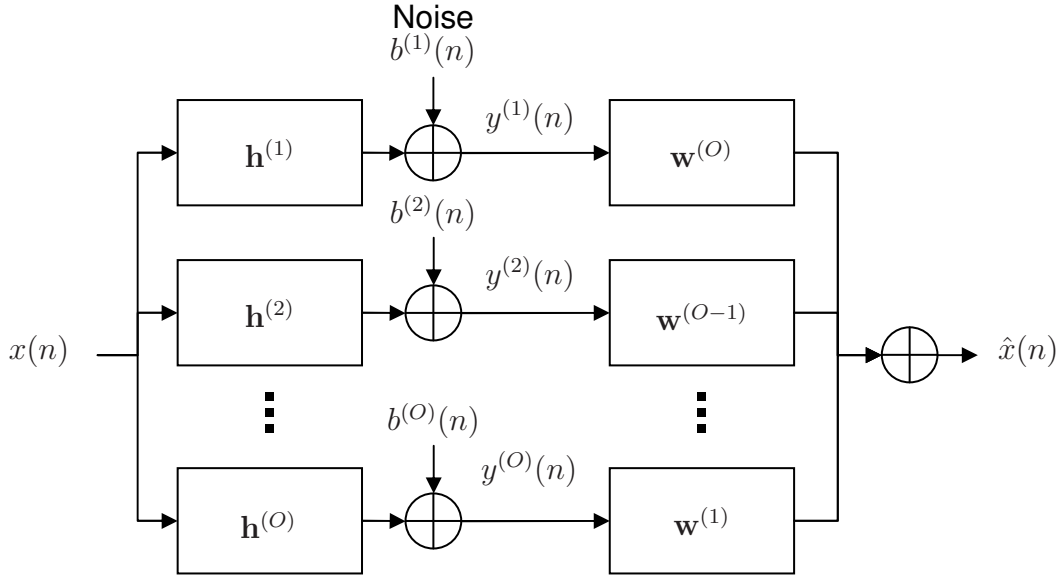
Figure 2.2:   Multichannel communications model   [8]

note that the baseband model presented in Figure 2.1 can equivalently be represented as a multiple channel system, with each of O subchannels consisting of T_{sym} spaced samples. This structure is shown in Figure 2.2. For modelling a communications system as a series of matrix computations, the effective channel impulse response can be represented as a convolutional matrix, and can aid in gaining an understanding of the equalization process. The following derivation of a matrix-focused model is derived from [6] and [10].

Each subchannel impulse response $h^{(i)}(n)$ and subchannel equalization filter $w^{(i)}(n)$ sequence can be defined as vectors shown in (2.8) and (2.9), where L is the effective channel length, M is the number of equalizer taps, and O is the oversampling factor.

$$\mathbf{h}^{(i)} = [h^{(i)}(0), \ h^{(i)}(1), \ ... \ h^{(i)}(L-1)]^T \ , \ i = 1, ..., O \tag{2.8}$$

$$\mathbf{w}^{(i)} = [w^{(i)}(0), \ w^{(i)}(1), \ ... \ w^{(i)}(M/O-1)]^T \ , \ i = 1, ..., O \tag{2.9}$$

10

These subchannel equalization vectors can then be combined and stacked column wise to form a single new vector $\mathbf{w}(n)$. This vector is formatted differently than the oversampled equalization vector $\mathbf{w}'$, and it is important to note that they are not equivalent.

$$\mathbf{w}(n) = \begin{bmatrix} \mathbf{w}^{(O)}(n) \\ \vdots \\ \mathbf{w}^{(1)}(n) \end{bmatrix} \tag{2.10}$$

The matched filter output at the receiver of each subchannel $y^{(i)}(n)$ can be expressed as a vector by recasting all of the previous discrete sequences as vectors or convolution matrices. Let $\mathbf{y}^{(i)}(n)$ be a vector of N samples at the matched filter output as shown in (2.11).

$$\mathbf{y}^{(i)}(n) = [y^{(i)}(n),\ y^{(i)}(n-1),\ y^{(i)}(n-2),\ ...\ y^{(i)}(n-N+1)]^T \tag{2.11}$$

The transmitted symbol vector $\mathbf{x}(n)$ and the subchannel AWGN noise vector, $\mathbf{b}^{(i)}(n)$, are defined similarly as shown in (2.12) and (2.13).

$$\mathbf{x}(n) = [x(n),\ x(n-1),\ x(n-2),\ ...\ x(n-N-L+2)]^T\ , \tag{2.12}$$

$$\mathbf{b}^{(i)}(n) = [b^{(i)}(n),\ b^{(i)}(n-1),\ b^{(i)}(n-2),\ ...\ b^{(i)}(n-N+1)]^T \tag{2.13}$$

The subchannel convolution matrix $\mathbf{H}_N^{(i)}$ for each subchannel is a Toeplitz matrix with the subchannel impulse response vector $\mathbf{h}^{(i)}$ along the first row as shown in (2.15). The convolution matrix for each subchannel acts on $(N-L-1)$ transmitted symbols in $\mathbf{x}(n)$ to provide N samples in the subchannel output vector $\mathbf{y}^{(i)}(n)$.

$$\mathbf{y}^{(i)}(n) = \mathbf{H}_N^{(i)}\mathbf{x}(n) + \mathbf{b}^{(i)}(n) \tag{2.14}$$

$$\mathbf{H}_N^{(i)} = \overbrace{\left.\begin{bmatrix} h^{(i)}(0) & \cdots & h^{(i)}(L-1) & 0 & \cdots & \cdots & 0 \\ 0 & h^{(i)}(0) & \cdots & h^{(i)}(L-1) & 0 & \cdots & 0 \\ \vdots & & & & & & \vdots \\ 0 & \cdots & \cdots & 0 & h^{(i)}(0) & \cdots & h^{(i)}(L-1) \end{bmatrix}\right\} N}^{N+L} \tag{2.15}$$

Stacking all subchannel vectors columnwise allows the entire multichannel output vector $\mathbf{y}(n)$ to be expressed in terms of the stacked convolution matrices of each subchannel:

$$\begin{aligned} \mathbf{y}(n) &= \begin{bmatrix} \mathbf{y}^{(1)}(n) \\ \vdots \\ \mathbf{y}^{(O)}(n) \end{bmatrix}, \\ &= \begin{bmatrix} \mathbf{H}_N^{(1)} \\ \vdots \\ \mathbf{H}_N^{(O)} \end{bmatrix} \mathbf{x}(n) + \begin{bmatrix} \mathbf{b}^{(1)}(n) \\ \vdots \\ \mathbf{b}^{(O)}(n) \end{bmatrix}, \\ &= \mathbf{H}_N \mathbf{x}(n) + \mathbf{b}(n) \end{aligned} \tag{2.16}$$

Similarly, each subchannel equalization filter $\mathbf{w}^{(i)}$ can be cast as a convolution matrix as in (2.15), shown in (2.17). Combining these convolutional matrices row-wise as shown in (2.18) provides a method to calculate an estimate of the transmitted vector $\hat{\mathbf{x}}(n)$, shown in (2.19).

12

$$\mathbf{W}_N^{(i)} = \overbrace{\begin{bmatrix} w^{(i)}(0) & \cdots & w^{(i)}(L-1) & 0 & \cdots & \cdots & 0 \\ 0 & w^{(i)}(0) & \cdots & w^{(i)}(L-1) & 0 & \cdots & 0 \\ \vdots & & & & & & \vdots \\ 0 & \cdots & \cdots & 0 & w^{(i)}(0) & \cdots & w^{(i)}(L-1) \end{bmatrix}}^{N+L} \left.\vphantom{\begin{bmatrix} \\ \\ \\ \\ \end{bmatrix}}\right\} N \tag{2.17}$$

$$\mathbf{W}_N = \begin{bmatrix} \mathbf{W}_N^{(O)} \cdots \mathbf{W}_N^{(1)} \end{bmatrix} \tag{2.18}$$

$$\hat{\mathbf{x}}(n) = \mathbf{W}_N \mathbf{y}(n) \tag{2.19}$$

2.4 Equalization Techniques

This section will examine the both the cooperative and non-cooperative equalizer algorithms used in this thesis, and provide an overview of the important characteristics of each. An overview of important equalization concepts is presented first, covering the broad types of equalizers and their strengths and weaknesses. The cooperative receiver structure used in this thesis is presented next, followed by an overview of non-cooperative or blind equalizers used.

2.4.1 Equalization Algorithm Characteristics. Blind equalization algorithms can be grouped into two broad categories: algorithms that are based on the estimation of a transmitted signal's second order statistics (SOS), and algorithms that calculate equalizer coefficients based on higher order statistics (HOS). As second order statistics can be accurately estimated over fewer observations, SOS algorithms typically converge faster than algorithms making use of HOS [5]. In a wireless transmission environment the channel conditions often vary over time, making algorithms with a

13

quick convergence rate desirable. If the channel conditions are changing more rapidly than an equalizer can track, then the equalizer is unable to invert the channel to cancel out multipath effects making data extraction difficult [18].

Equalizers can also be classified by the sampling rate used. An algorithm typically either uses a single sample from each communications symbol in a transmitted signal, or multiple samples from each symbol. Algorithms using multiple samples from each transmitted symbol are known as fractionally spaced equalizers (FSE), while algorithms using a single sample are known as sample or baud spaced equalizers (BSE). Fractionally spaced equalizer algorithms typically perform better than equivalent BSE methods [14], converging faster and more accurately [5].

Another classification parameter worth considering is an algorithm's ability to adapt its equalizer coefficients. As stated above, the wireless transmission environment often includes time varying channel conditions. Algorithms that update the equalization filter after every received symbol are known as continuously adaptive. Algorithms which process a block or group of symbols before calculating an equalization filter are known as periodically adaptive. An algorithm can also be either a direct equalization method or and indirect equalization method. A direct method calculates the filter taps for a linear equalization filter which is then applied, where an indirect filter estimates the channel impulse response before attempting to calculate an equalization filter.

2.4.2 Minimum Mean Square Error (MMSE) Equalization . The cooperative equalizer used in this thesis is an example of a minimum mean squared error (MMSE) equalizer, based on the derivation in [12]. This MMSE equalizer attempts to minimize the cost function $J(n)$ shown in (2.20),

14

$$J(n) = \mathrm{E}\left[x^*(n-\delta)x(n-\delta)\right] - 2\mathrm{Re}\left\{\mathrm{E}\left[x(n-\delta)\mathbf{y}^H(n)\right]\mathbf{w}^*\right\}$$
$$+ \mathbf{w}^T\mathrm{E}\left[\mathbf{y}(n)\mathbf{y}^H(n)\right]\mathbf{w}^*$$
$$= \mathrm{E}\left[x^*(n-\delta)x(n-\delta)\right] - 2\mathrm{Re}\left\{\mathbf{p}_{xy}^T\mathbf{w}^*\right\} + \mathbf{w}^T\mathbf{R}_y\mathbf{w}^* \qquad (2.20)$$

where $\mathbf{w}$ is the equalization filter, $\mathbf{R}_y$ is the autocorrelation function of the received vector, and $\mathbf{p}_{xy}$ is the cross correlation of the transmitted and received signals. Setting the cost function gradient given in (2.21) to zero allows for the optimal mean squared error equalization filter to be calculated exactly according to (2.22).

$$\nabla_{\mathbf{w}}J(n) = -2\mathbf{p}_{xy}^T + 2\mathbf{w}^T\mathbf{R}_y \qquad (2.21)$$

$$\mathbf{w}_{opt} = \left(\mathbf{R}_y^T\right)^{-1}\mathbf{p}_{xy} \qquad (2.22)$$

In a cooperative receiver context, the autocorrelation and cross correlation matrices, $\mathbf{R}_y$ and $\mathbf{p}_{xy}$ respectively are easily calculated, and the implementation of this cooperative method in this thesis in the presence of timing dither and multipath is presented in Chapter 3.

2.4.3 Constant Modulus Algorithm (CMA) Equalization .   The constant modulus algorithm (CMA) is a very common blind equalization technique [6], and both baud and fractionally spaced versions have been studied and documented extensively in literature. CMA uses higher-order statistics to directly and adaptively equalize the channel, and the fractionally spaced version provides perfect equalization under noiseless conditions for most channels [6]. The baud spaced version of CMA, indeed any BSE, requires an infinite equalizer filter length to achieve perfect equalization, making it somewhat impractical [4].

15

CMA works by minimizing an error term $e(n)$ calculated by taking the difference between the expected average amplitude and the sampled magnitude of a symbol, as shown in (2.23).

$$e(n) = \frac{\mathrm{E}\left[|x(n)|^4\right]}{\mathrm{E}\left[|x(n)|^2\right]} - |\hat{x}(n)|^2 \tag{2.23}$$

The error term can be minimized using the update strategy shown in (2.24), where μ is the convergence step size of the algorithm, $\mathbf{w}(n)$ is the equalizer coefficient vector, and $\mathbf{y}^*(n)$ is a regressed vector of the received symbol samples. In effect, the CMA algorithm updates its nth equalizer filter tap by operating on a range of received symbols.

$$\begin{aligned} \mathbf{w}(n+1) &= \mathbf{w}(n) + \mu\mathbf{y}^*(n)\left(x(n) - \mathbf{y}^T(n)\mathbf{w}(n)\right) , \\ &= \mathbf{w}(n) + \mu\mathbf{y}^*(n)e(n) . \end{aligned} \tag{2.24}$$

Being a minimization acting on the square of the error term, $e(n)$, which also contains the squared symbol estimate, the convergence of CMA relies on the estimation of fourth order statistics. This dependence causes CMA to have a low convergence speed when compared to SOS based algorithms [5]. If the signal is constant modulus, meaning that each symbol has the same amount of energy, the error term approaches zero as the equalization filter converges. The CMA algorithm will also converge for non constant modulus signal constellations, but will converge much more slowly due to the cost surface having a non-zero minima [6].

CMA assumes a wide sense stationary (WSS) or cyclostationary received signal; WSS for a baud spaced implementation and cyclostationary for a FSE implementation. Under time varying channel conditions these assumptions will be violated, but if the channel impulse response varies slowly enough, the statistics of the signal may still be stable enough for CMA to equalize the channel [5]. In FSE CMA, four conditions

16

are needed to guarantee equalizer filter coefficients that perfectly equalize the channel impulse response. First, the channel must be noiseless. The source signal must be a series of independent and identical symbols selected from a circularly symmetric constellation, and the kurtosis of the symbol distribution must be less than the kurtosis of a Gaussian distribution [6]. Also, the channel convolution matrix defined by Tong *et al.* in [16] must be full column rank.

The full column rank condition for perfect equalization leads to a minimum number of equalizer filter taps required in implementing the CMA algorithm. The number of taps needed is a function of the length of the channel response and the number of samples taken per symbol, or the sampling rate, and is shown in (2.25)

$$M \geq L + \frac{M}{O} - 1 \tag{2.25}$$

where M is the number of equalization filter taps, L is the effective length of the channel impulse response, and O is the oversampling factor [6].

2.5 Multipath

Multipath interference is an issue that commonly arises in wireless communications. A large body of research exists on the cancellation and equalization of multipath interference, but this thesis examines the effects of this interference on an ISI time dithered transmitter and receiver pair. This ISI waveform necessitates a new receiver structure design for acceptable demodulation. This section begins with a discussion of the causes of multipath interference, introduces some of the differing effects and systems that can be affected, and presents some possible models that can be adapted to the ISI multipath problem at hand.

As the name implies, multipath interference is caused by having multiple time delayed versions of a transmitted signal arriving at the receiver as a result of the transmission taking several different paths. This can affect many different systems, but radio or wireless transmission media typically have the worst problem with mul-

tipath due to the difficulty in focusing all of the transmitted energy along a single path [3]. Table 2.1 summarizes the mechanisms involved in the observed multipath effects of several different systems.

Table 2.1:   Multipath mechanisms [3]

System	Multipath mechanism
HF Radio	Reflection from multiple ionospheric layers
Mobile and personal radio	Reflection and scattering from buildings, etc
Microwave point to point links	Atmospheric refraction and reflection
Satellite-mobile systems	Ground and building reflection
Radio LAN/indoor radio	Reflections from walls and building structure
Diffuse infrared	Reflections from walls
Multimode optical fibre	Multimode propogation
Telephone/cable network	Reflections from terminations

There are several factors influencing the amount of multipath interference present in any system, and the steps needed to attempt to equalize it. The first area to consider is the characteristics of the physical transmission channel. The geography of the transmission area may hold tall buildings, water towers, and other obstacles that would reflect the transmitted signal and create a delayed version at the receiver [2]. If a strong line of sight (LOS) path is present in the channel, the presence of such a path simplifies the equalization problem, but in some environments such as in urban areas the LOS path is often blocked or obscured by surrounding buildings. If the transmitter or receiver are moving relative to one another, then any multipath reflections present will have time-varying delays at the receiver. These time delays will affect the phase of the transmitted multipath signal with respect to the original transmission, and result in phase distortion. The distance between the transmitter and receiver plays a factor, as the signal suffers free space path loss attenuation according to the $1/d^2$ law [2]. Even the characteristics of the objects in the transmission environments can have an effect. Some objects, such a a metallic water tower, will reflect more of the transmitted energy than a stone building, resulting in a multipath containing more of the original signal power. This is known as the *reflectivity* property of the object. In general, a transmission environment that is *stationary*, meaning that the

18

transmitter/receiver pair and objects in the environment are not moving, is easier to equalize at the receiver than time-varying multipath conditions.

2.5.1 Multipath Modelling. In order to develop a model for multipath interference for use in simulations, the following derivation is presented based upon the development in [13]. First, consider a transmitted signal $s(t)$ modulated at a carrier frequency f_c consisting of a series of extremely short pulses. $s(t)$ takes the form shown in (2.26)

$$s(t) = \Re\left[s_l(t)e^{j2\pi f_c t}\right] \tag{2.26}$$

where $s_l(t)$ represents the baseband transmitted signal, or the signal before modulation. After transmission, multiple propagation paths are assumed, and each path has an associated attenuation factor, $\alpha_n(t)$ and delay term, $\tau_n(t)$. Both of these factors are dependent on time due to the varying nature of the transmission environment [13]. The received bandpass signal at the receiver $x(t)$ is given in (2.27).

$$x(t) = \sum_n \alpha_n(t)s(t - \tau_n(t)) \tag{2.27}$$

Substituting $s(t)$ from (2.26) into (2.27) yields the new complete form of $x(t)$

$$x(t) = \Re\left\{\left[\sum_n \alpha_n(t)e^{-j2\pi f_c \tau_n(t)}s_l(t - \tau_n(t))\right]e^{j2\pi f_c t}\right\} \tag{2.28}$$

representing the complete model of the received bandpass signal. By applying lowpass filtering to $x(t)$ as shown in (2.28), the lowpass received signal $r_l(t)$ can be written equivalently as (2.29).

$$r_l(t) = \sum_n \alpha_n(t)e^{-j2\pi f_c \tau_n(t)}s_l(t - \tau_n(t)) \tag{2.29}$$

19

Since $r_l(t)$ is the response of a lowpass channel to the equivalent lowpass signal, $s_l(t)$, the lowpass channel can be described by the time variant impulse response given in (2.30) [13]. This also represents the multipath channel, $h_{phys}^{(ct)}(t)$, as given in (2.2).

$$c(\tau; t) = \sum_n \alpha_n(t) e^{-j2\pi f_c \tau_n(t)} \delta(\tau - \tau_n(t)) \tag{2.30}$$

Assuming the lowpass channel impulse response $c(\tau; t)$ is wide sense stationary (WSS), the the autocorrelation function of $c(\tau; t)$ is defined as ϕ_c.

$$\phi_c(\tau_1, \tau_2; \Delta t) = \frac{1}{2} E\left[c^*(\tau_1; t) c(\tau_2; t + \Delta t)\right] \tag{2.31}$$

As each propagation path passes through a different transmission environment, each is subject to different attenuations and phase shifts. In most wireless transmission media, these attenuations and phase shifts are uncorrelated with one another [13]. Assuming these factors are uncorrelated for two different delays, ϕ_c can be written as shown in (2.32).

$$\frac{1}{2} E\left[c^*(\tau_1; t) c(\tau_2; t + \Delta t)\right] = \phi_c(\tau_1; \Delta t)\delta(\tau_1 - \tau_2) \tag{2.32}$$

Letting $\Delta t = 0$, the autocorrelation function $\phi_c(\tau; 0)$, or $\phi_c(\tau)$, is the average power output of the channel as a function of time. As such, $\phi_c(\tau)$ is known as the multipath intensity profile of the channel [13]. In many typical systems, the measured $\phi_c(\tau)$ appears as shown in Figure 2.3. Physically, this represents the expected power of a multipath coefficent of a channel at a particular delay τ.

2.6 Dither Algorithm

This section provides an overview of the method developed in [8] to induce time varying ISI into a transmitted waveform to make it difficult to equalize. As the equalization techniques discussed in Section 2.4 all rely on a slowly changing effective
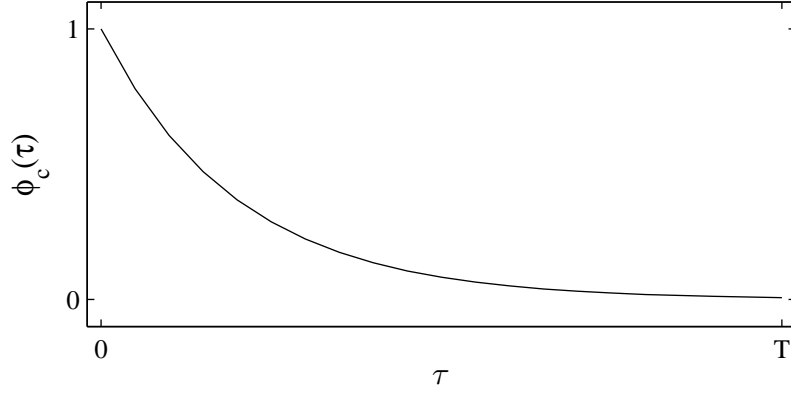
Figure 2.3:   Typical Multipath Intensity Profile

channel impulse response, any ISI injected will have to be severe enough to prevent third party demodulation. The time varying aspect of the induced ISI must be large enough to frustrate blind equalization techniques as well, but not so severe as to prevent effective cooperative equalization.

Most traditional receivers transmit one symbol at a time, with each new symbol beginning at some set time spacing, T_{sym}, as stated in Section 2.3. To create the ISI in the waveform, the beginning of each symbol is delayed within the range of T_{sym}. The dither waveform can then be pictured as a series of T_{sym} time blocks which each contain the leading edge of exactly one communications symbol. This limitation preserves the traditional transmission symbol rate, and simplifies the design of a cooperative receiver [8].

This delay is applied to the transmitted waveform immediately after the DAC, as shown in Figure 2.4, with the delay of a particular symbol n from the start of the nth T_{sym} and is defined as $d(n)$. After the application of this dither, the transmitted signal $x^{(ct)}(t)$ is expressed in (2.33)

$$x^{(ct)}(t) = \sum_{n=0}^{N-1} x(n)\delta\left(t - nT_{sym} - d(n)\right) , \qquad (2.33)$$

where $x(n)$ is the transmitted data symbols, and $d(n)$ is a sample of a random variable D. D is a uniform random variable with probability density function of $p_D^{(ct)}(t)$.

21
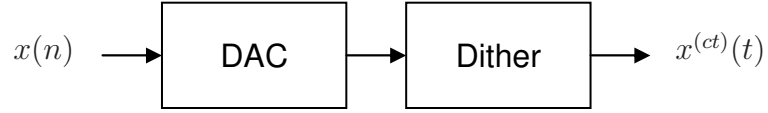
Figure 2.4:   A dither block in the transmitter creates ISI [8]

The range, T_{max}, of the uniform random variable D can be selected, so long as it falls within $[0, T_{sym}]$. The probability density function can be written in terms of the selected range T_{max} as shown in (2.34).

$$p_D^{(ct)}(t) = \begin{cases} 1/T_{max}, 0 \leq t < T_{max} \\ 0, \quad\quad t < 0 \text{ or } t \geq T_{max} \end{cases} \tag{2.34}$$

To create a sequence of pseudorandom delays $d(n)$, each individual delay must be selected from a discrete set of possible delays. Based on a uniform distribution, the symbol period is divided into $P + 1$ equally spaced possible delay values. The discrete probability density function $P_D(t)$ is given in (2.35)

$$p_D(t) = \frac{1}{p_{max} + 1} \sum_{p=0}^{p_{max}} \delta\left(t - \frac{pT_{sym}}{P}\right), \tag{2.35}$$

where p_{max} is the largest integer delay value contained within T_{max}. The relationship between p_{max} and T_{max} is given in (2.36), where $\lfloor\rfloor$ is the floor function which rounds down to the largest integer value.

$$p_{max} = \left\lfloor \frac{PT_{max}}{T_{sym}} \right\rfloor \tag{2.36}$$

As a finite sequence, the delay code $d(n)$ will have some associated period, N_d. In all cases, this thesis considers long delay codes with periods larger than the number of transmitted data symbols. It is also possible to develop cooperative receivers that can function provided a short period code is used relative to the number of transmitted symbols available for equalizer training [8], but the performance of such a receiver in the presence of multipath is not examined in this thesis. Excluding the effects of

22

multipath interference, the severity of the ISI created through the dither process is a function of the pulse shape characteristics and the range of T_{sym} over which the delay probability density function is allowed to use, T_{max}. In this thesis various fixed pulse shapes will be used with varying symbol dither to characterize the non-cooperative suppression capabilities of the developed dither algorithm in the presence of multipath interference.

23

III. Research Methodology

3.1 Overview

This chapter presents a numerical simulation method for testing the performance of the ISI algorithm reviewed in Section 2.6, in the presence of multipath interference. Section 3.2 introduces the overall model used to build up the simulation designed and implemented in MATLAB, with Sections 3.3, 3.4, and 3.5 discussing the transmitter model, the channel model, and the receiver model respectively. The binary DPSK constellation used in this thesis is detailed in Section 3.3, along with the pulse shapes used for the communications symbols. A derivation of the multipath interference models is provided in Section 3.4, and Section 3.5 includes derivations of how the equalization models reviewed in Chapter II are implemented in simulation. Section 3.6 provides a progressive validation of the different components of the numerical simulation model.

3.2 Model Overview

The end-to-end complete communications system modeled in Matlab in this thesis is shown in Figure 3.1. The transmitter block takes the input bit stream b_{in} and creates a baseband waveform of binary DPSK symbols. The channel block injects AWGN and multipath interference effects into the waveform, and the receiver block estimates the transmitted symbols to produce the output bit sequence b_{out}. As the intent of this thesis is to examine the performance of the dither algorithm developed in [8], the original transmitter structure remains unchanged. The channel model and correspondingly the receiver models have been adapted to include multipath interference explicitly as detailed in the corresponding sections below.

$\{b_{in}\} \longrightarrow$ Transmitter $\longrightarrow$ Channel $\longrightarrow$ Receiver $\longrightarrow$ $\{b_{out}\}$

Figure 3.1:   Simulation Block Diagram [8]

24

3.3   Transmitter Model

The transmitter block diagram shown in Figure 3.2 details the steps involved in creating the sampled transmitted waveform, $u(p)$. The simulation uses binary DPSK modulation to encode the input bit sequence into a series of symbols.
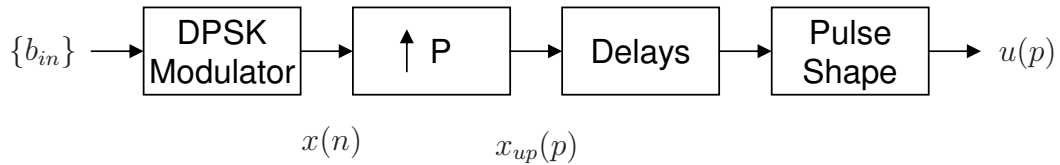
Figure 3.2:   Simulated transmitter block diagram [8]

The DPSK modulation is circularly symmetric about the origin in the signal or constellation space, with equal magnitude symbols and uniform phase separation between symbols. In DPSK, a constellation of M symbols is separated into a series of words of length l, where $l=log_2(M)$ bits. These l bit words are mapped to a phase offset using Gray coding. Figure 3.3 shows the binary DPSK constellation, and Table 3.1 provides the corresponding Gray code symbol mapping [14]. Binary DPSK also satisfies the conditions for perfect equalization of the CMA algorithm as discussed in Chapter II.

Figure 3.3:   Binary DPSK Constellation

The upsampling block increases the sampling frequency by oversampling by a factor of P, (P=64 throughout this thesis) placing an integer number of zero valued samples between each transmitted symbol. The signal is now a sequence of symbols

25

Table 3.1:   Binary DPSK Gray code mapping

Binary	
Word	Phase Shift, $\Delta\theta$
0	0
1	π

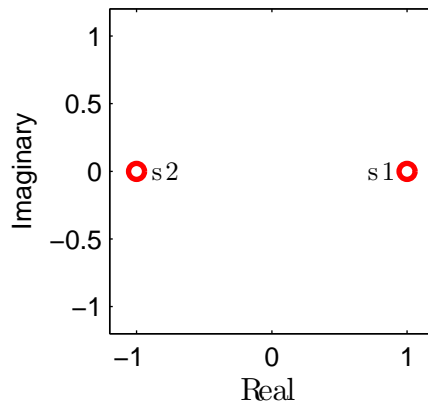spaced P samples apart. An upsampling factor of 64 is used throughout this thesis. Upsampled signals are indexed using the parameter p. Two variables are used for upsampling and downsampling in this thesis: P and O. These two different variables are used to model a continuous time signal using a discrete time model. Upsampling by P ensures that the continuous time signal is sampled at a high enough rate to approximate the signal digitally. The downsampling factor O is used in the receiver to downsample the signal by 32 to make use of $T_{sym}/2$ fractionally spaced equalizers. This downsampling factor could be any value equal or less than 64, but fractionally spaced equalizers provide a good tradeoff in saved complexity and equalizer performance. The delay block implements the symbol timing dither algorithm overviewed in Section 2.6, moving each impulse an integer number of samples as specified by the delay code. To implement the symbol dither, the dither algorithm generates a pseudo-random delay code **d** consisting of integer delays to be applied to each corresponding symbol. The maximum allowable delay must be less than P-1 samples to prevent transmitting symbols out of order. The distribution of delays is uniform across the maximum allowable delay period throughout this thesis, and this maximum delay term can be adjusted to limit the amount of ISI induced in the transmitted waveform. The signal is then convolved with the pulse shape signal $f(p)$ to produce the transmitted waveform $u(p)$.

3.3.1 Pulse Shape.   This thesis uses a Square Root Raised Cosine (SRRC) pulse shape, with several different roll off factors β. The β value measures the amount of energy that is in the additional lobes of the SRRC shape, with lower beta values having more energy outside the main lobe. Figure 3.4, shows the three SRRC shapes used in this thesis. As the SRRC pulse shape is unbounded, it must be truncated in

26

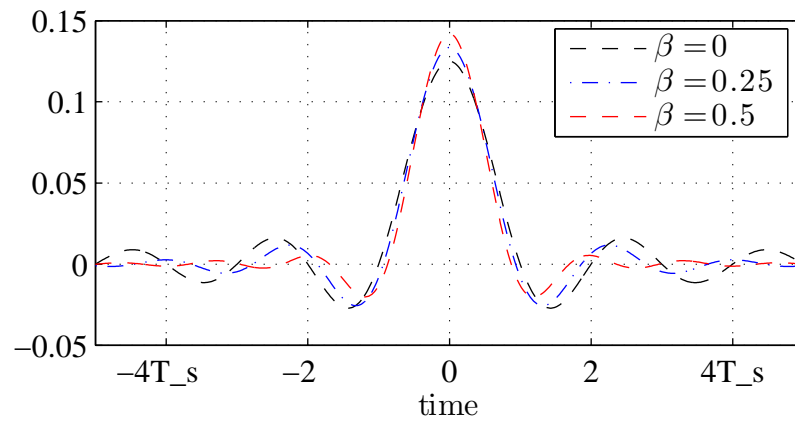any physical system. Throughout this thesis, the SRRC pulse width pw is 10 symbol periods wide centered at t=0.

Figure 3.4:   SRRC pulseshapes with β=0, 0.25 & 0.5

27

3.4   Channel Model

The simulated physical channel used in this thesis is a combination of the multipath conditions present in the channel (h_{phys}) and an AWGN noise signal $\nu(p)$ as shown in Figure 3.5.
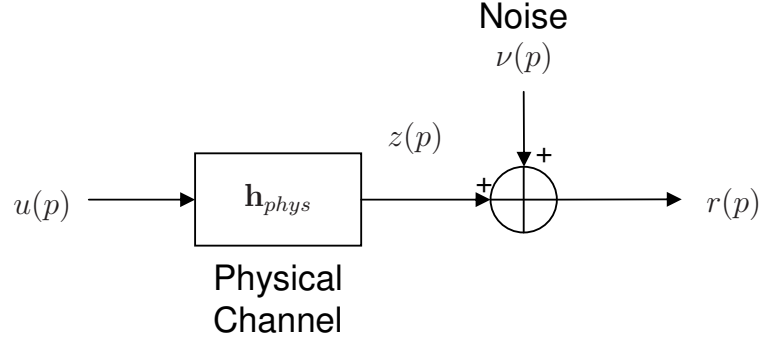
Figure 3.5:   Simulated channel block diagram [8]

After applying the multipath effects of the channel, the AWGN signal is added. The noise samples are complex, with the real and imaginary components of each sample having independent Gaussian distributions. The noise sample variances are then scaled to achieve a desired SNR at the input of the receiver, and are expressed in terms of E_b/N_o. This simulated SNR is calculated using the mean squares of the transmitted signal $z(p)$ and the noise signal $\nu(p)$ as shown in (3.1)

$$SNR \approx \frac{\sum |z(p)|^2}{\sum |\nu(p)|^2} \ . \tag{3.1}$$

It is also important to note that in the presence of ISI due to symbol timing dither, pulse shapes, and multipath conditions can be treated as a noise source. These are not included in SNR calculations in this thesis. The multipath interference models used and their implications are discussed in Section 3.4.1.

28

3.4.1 Multipath Model. The purpose of this thesis is to examine the performance of a symbol timing dither waveform in the presence of multipath interference. In order to do that, two separate multipath profile models are presented here. The first is composed of a line-of-sight path modeled with zero delay and one multipath reflection delayed $3T_{sym}$, the second consists of a line-of-sight path with zero delay and 3 multipath reflections, at $2T_{sym}$, $4T_{sym}$ and $6T_{sym}$ delays, respectively. In order to provide diversity in the multipath modelling, 50 distinct channels are generated for both the 2 and 4 ray models. Each of these channels is randomly generated by defining a deterministic delay profile based on (3.2)

$$j(t) = e^{-\alpha t} \tag{3.2}$$

where α represents a scalar modeling the rate of exponential decay [7]. For the 2 ray model, the line-of-sight channel's amplitude is defined as yielding unity power, and the multipath reflection power is $\sqrt{0.35}$. For the 4 ray model, the three multipath reflections have power values of $\sqrt{0.22}$, $\sqrt{0.05}$, $\sqrt{0.02}$, respectively. These choices are consistent with the typical multipath intensity profile, shown in Figure 2.3. Each multipath reflection power value is then multiplied by a zero mean unit variance Gaussian random variable. This generates 50 unique channels for each multipath model, where each multipath reflection is normally distributed with the average power value selected above. The delays between multipath reflections is held constant for all simulations of a given model throughout this thesis. Each channel is then normalized to unity power to prevent adding any artificial power to the system through the multipath interference. To produce results reflecting the average performance of a symbol timing dither waveform in multipath, the simulation transmits $N=1000$ symbols for training the CMA equalizer, and $N=1000$ symbols for estimation using each of these random channels in turn as h_{phys}. The bit error rate (BER), P_b is calculated over each channel and averaged together to provide the final results, presented in Chapter IV. Definitions for P_b used in this thesis are provided in Section 3.5.
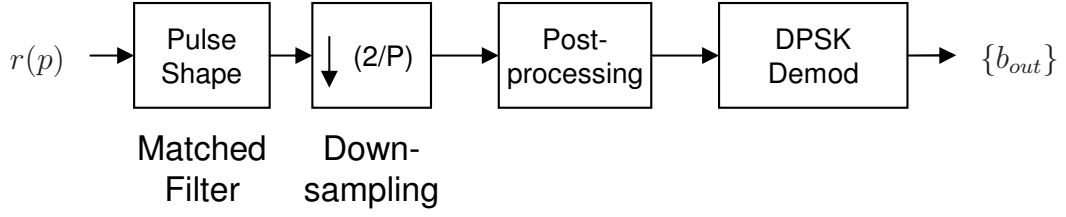
29

Figure 3.6:   Simulated receiver block diagram [8]

3.5   Receiver Model

The simulated receiver block diagram is shown in Figure 3.6. The receiver takes the input received signal $r(p)$ and convolves it with the same pulse shape used in the transmitter block. This applies the effects of matched filtering at the receiver. The resulting signal is then downsampled by a factor of $2/P$. This results in having 2 samples from every transmitted symbol period, enabling fractionally spaced equalization using two subchannels in both the cooperative MMSE and non-cooperative CMA algorithms presented in this thesis. The baseline symbol spaced receiver only uses data from the first subchannel, which is analogous to symbol spaced sampling. This simulation synchronizes the first subchannel to the point of the maximum effective channel impulse response in the absence of symbol timing dither. This provides the highest SNR values for the basic symbol spaced receiver. In the presence of symbol timing dither, the simulation synchronizes to the point of the average maximum effective channel response within the symbol period.

The binary DPSK demodulator uses the phase difference between the current symbol and the previous estimated symbol to estimate transmitted information bits. Because this process is dependent only on the phase difference between adjacent estimated symbols and not the absolute phase values, this technique is immune to rotation of the constellation in the signal space [14]. For DPSK, the probability of bit error is

$$P_b = \frac{1}{2} e^{\frac{-E_b}{N_o}} \tag{3.3}$$

30

where E_b is the average energy per bit in the information signal and N_o is the noise power spectral density. All analytical P_b curves presented in this thesis are generated using (3.3).

3.5.1 Cooperative Receiver. In a known channel, MSE minimization is a common approach for calculating an equalization filter to deconvolve channel effects. Given a constant or static channel impulse response, the MSE minimization process produces one single equalization filter. As the multipath interference present in a channel is held constant for the purposes of equalization in this simulation, the multipath aspect of the channel is stable. However, in the presence of symbol timing dither, each element of the delay code will constitute a unique channel to equalize, necessitating the computation of N_d equalizers.

The basic structure of the MSE algorithm is presented in Section 2.4.2, with the optimal MSE equalization filter given by (2.22). In adapting the MSE algorithm for use in a pseudorandom delay waveform with multipath, a fractionally spaced implementation is used. To signify the ISI caused by the symbol timing dither, let $\mathbf{H}_N(n)$ represent the convolution matrix that will map the transmitted symbols, $\mathbf{x}(n)$ to the output vector $\mathbf{y}(n)$, similar to the formation shown in (2.16). As each symbol can potentially have a unique delay due to the symbol timing dither, the convolution matrix must also be indexed by n.

The autocorrelation of the output signal is given in (3.4), and is also dependent upon the symbol timing dither applied to each symbol and is indexed by n.

$$
\begin{aligned}
\mathbf{R}_y(n) &= E\left[\mathbf{y}(n)\mathbf{y}^H(n)\right] \ , \\
&= E\left[\left(\mathbf{H}_N(n)\mathbf{x}(n) + \mathbf{b}(n)\right)\left(\mathbf{H}_N(n)\mathbf{x}(n) + \mathbf{b}(n)\right)^H\right] \ , \\
&= E\left[\mathbf{H}_N(n)\mathbf{x}(n)\mathbf{x}^H(n)\mathbf{H}_N^H(n)\right] + E\left[\mathbf{b}(n)\mathbf{b}^H(n)\right] \ , \\
&= \mathbf{H}_N(n)\mathbf{R}_x\mathbf{H}_N^H(n) + \mathbf{R}_b \ .
\end{aligned}
\tag{3.4}
$$

Again, the cross-correlation vector $\mathbf{p}_{xy}(n)$ is dependent on the symbol index n:

$$\begin{aligned}
\mathbf{p}_{xy}(n) &= E\left[\mathbf{y}^*(n)x(n-\delta)\right] , \\
&= E\left[\left(\mathbf{H}_N(n)\mathbf{x}(n) + \mathbf{b}(n)\right)^* x(n-\delta)\right] , \\
&= \mathbf{H}_N^*(n)E\left[\mathbf{x}^*(n)x(n-\delta)\right] .
\end{aligned} \tag{3.5}$$

Finally, the MSE optimal filter must now indexed as well:

$$\mathbf{w}_{opt}(n) = \left(\mathbf{R}_y^T(n)\right)^{-1}\mathbf{p}_{xy}(n) . \tag{3.6}$$

Equation (3.6) shows the form of the optimal MSE filter that must be calculated for each symbol. In order to calculate the optimal filter, the terms defining $\mathbf{R}_y(n)$ and $\mathbf{p}_{xy}(n)$, namely $\mathbf{H}_N(n)$, $\mathbf{R}_x$, $\mathbf{R}_b$, and $E\left[\mathbf{x}^*(n)x(n-\delta)\right]$ must be defined. Based on the derivations found in Section 3.2.2 of [8], these parameters are presented below.

$\mathbf{H}_N^{(i)}(n) =$

$$\overbrace{\begin{bmatrix}
h_n^{(i)}(0) & \cdots & h_{n-L+1}^{(i)}(L-1) & 0 & \cdots & \cdots & 0 \\
0 & h_{n-1}^{(i)}(0) & \cdots & h_{n-L}^{(i)}(L-1) & 0 & \cdots & 0 \\
\vdots & & & & & & \vdots \\
0 & \cdots & \cdots & 0 & h_{n-N+1}^{(i)}(0) & \cdots & h_{n-N-L+2}^{(i)}(L-1)
\end{bmatrix}}^{N+L} \left.\vphantom{\begin{bmatrix}1\\1\\1\\1\end{bmatrix}}\right\} N \tag{3.7}$$

Equation (3.7) represents the subchannel convolution matrix for a particular symbol n. Each row contained in $\mathbf{H}_N^{(i)}(n)$ is constructed from h_{eff} as given by 2.2, where h_{phys} includes the effect of the selected multipath interference channel. These rows also account for the ISI generated by nearby symbols on the symbol of interest n due to symbol timing dither. Each pulse shape is 10 symbol periods wide, so a window of n-5 to n+5 symbols could potentially influence the nth symbol. The convolution matrix $\mathbf{H}_N(n)$ is constructed by stacking the subchannel matrices for each symbol columnwise.

32

Assuming the source sequence $x(n)$ is zero mean and ideally and identically distributed, $\mathbf{R}_x$ is an identity matrix scaled by $E[x^*(n)x(n)]$ and $E[\mathbf{x}^*(n)x(n-\delta)]$ has precisely one nonzero element valued as $E[x^*(n)x(n)]$ at the $(\delta+1)$ element.

The elements discrete sampled elements of $\mathbf{R}_b$ can be defined as in (3.8)

$$E[b'(k_1)b'^*(k_2)] = N_o g^{(ct)}[(n_2 - n_1)T_{sym} + (i_2 - i_1)T_{sym}/O] \tag{3.8}$$

where $g^{(ct)}(t)$ represents the convolution of the pulse shape and multipath effects and the corresponding matched filter scaled by the noise power density, N_o.

$$\begin{aligned} g^{(ct)}(t) &= f^{(ct)}(t) \star f^{(ct)*}(-t) \\ &= \int_{-\infty}^{\infty} f^{(ct)}(\tau) f^{(ct)*}(t+\tau)\, d\tau \end{aligned} \tag{3.9}$$

These parameters can then be used with (3.6) to calculate each of the N_d necessary equalization filters for a particular delay code. As long as the multipath profile and the delay code remain the same, these N_d equalization filters can be reused assuming synchronization is maintained. The calculation of each optimal filter requires that the cooperative system have full knowledge of the pseudorandom delay sequence used and the multipath conditions present in the channel. As the multipath conditions in the channel can be measured before actual transmission using a training signal, this is feasible. Also, the equalizer must have some set delay built into the process, i.e. the estimated symbol $\hat{x}(n-\delta)$ is produced by the corresponding filter $\mathbf{w}_{opt}(n)$.

3.5.2 Non-Cooperative Receivers. There are two non-cooperative receiver structures presented in this thesis: a baseline symbol spaced receiver and a fractionally spaced CMA equalizer. Both are assumed to have knowledge of the symbol constellation, symbol period and the transmitted pulse shape, but have no knowledge

of the pseudorandom symbol timing delay values provided in $d(n)$. The performance of both equalizers in the presence of multipath and symbol timing dither is used to compare performance with the MMSE cooperative equalizer.

The basic receiver samples the matched filter output at the receiver at a rate of $1/T_{sym}$. This is analogous to symbol or baud spaced sampling. The bit error rate results of this receiver form a baseline for comparison of the other equalizer structures in the presence of multipath and symbol timing dither; as no equalization is performed, both the cooperative and non-cooperative equalization methods should best this baseline performance.

The FSE CMA equalizer utilizes the Constant Modulus Algorithm with a fractionally spaced implementation, i.e., the matched filter is sampled at $2/T_{sym}$. The CMA equalizer sampling phase is also synchronized as in the basic receiver. CMA equalization is detailed in Section 2.4.3. The CMA algorithm requires that the oversampled matched filter outputs be cyclostationary for perfect equalization, which is invalidated through the ISI induced by the presence of symbol timing dither. However, the adaptive nature of the CMA algorithm could still lead to improved bit error rate performance through equalizing the average ISI due to multipath and symbol timing dither conditions.

3.6   Simulation Validation

This section presents the validation process results. Each figure presented in this section is generated using the deterministic base multipath models, and include no randomized multipath channels as described in Section 3.4.1. Each P_b data point is generated using 50,000 symbols for estimation. All confidence intervals shown in the validation curves are 95% confidence intervals based on the number of bit errors, approximating Monte Carlo simulation methods.

3.6.1   Assumptions.   This section points out the assumptions and simplifications present in this simulation. Doppler effects are not modeled in this simulation, as the frequency of the carrier is assumed to be equal for each multipath reflection.

The receiver is capable of finding the point at which the combined channel impulse response is at a maximum and synchronizes to sample the waveform at this point. This synchronization is critical to the performance of the basic symbol spaced receiver structure. After the pseudorandom symbol timing dither is included in the system, the point at which this maximum occurs changes from symbol to symbol. The receiver will then synchronize to the average time in each symbol period at which the impulse response is at a maximum. This synchronization effect is applied within the simulation, and is assumed to be ideal.

The cooperative MMSE equalizer structure requires knowledge of the AWGN noise power. In simulation this is determined directly using the variance of the noise signal. In practice, the noise signal would not be available separate from the transmitted signal at the receiver, but this could be achieved in practice by determining the noise power at the receiver before transmission begins.
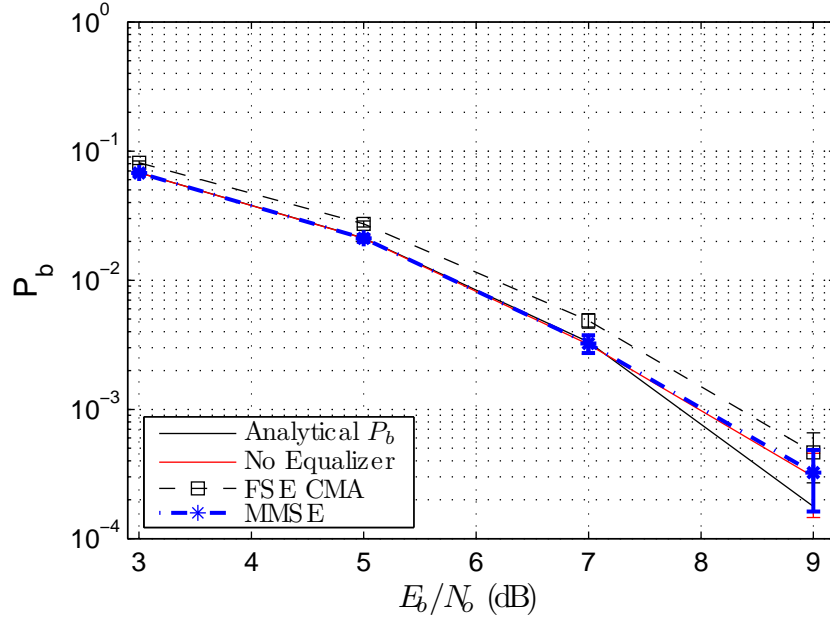
Figure 3.7:   Validation with no timing dither and SRRC β=0.25

Figure 3.7 represents a baseline simulation to test model validity. No multipath or symbol timing dither effects are included, and the analytical P_b is derived from the ideal binary DPSK performance curves as defined in [14]. All equalization methods are statistically identical to the analytical P_b curve under these conditions, as expected for a valid simulation model.

Figure 3.8 introduces symbol timing dither to the system, with a max timing delay of $0.6T_{sym}$. The symbol timing dither will create ISI in the system, degrading the performance of all equalizers. As the cooperative MMSE equalizer uses knowledge of the pseudorandom delay code generating the symbol timing delays, it performs better in terms of bit error rate than both the basic symbol spaced receiver and the non-cooperative CMA algorithm equalizer.
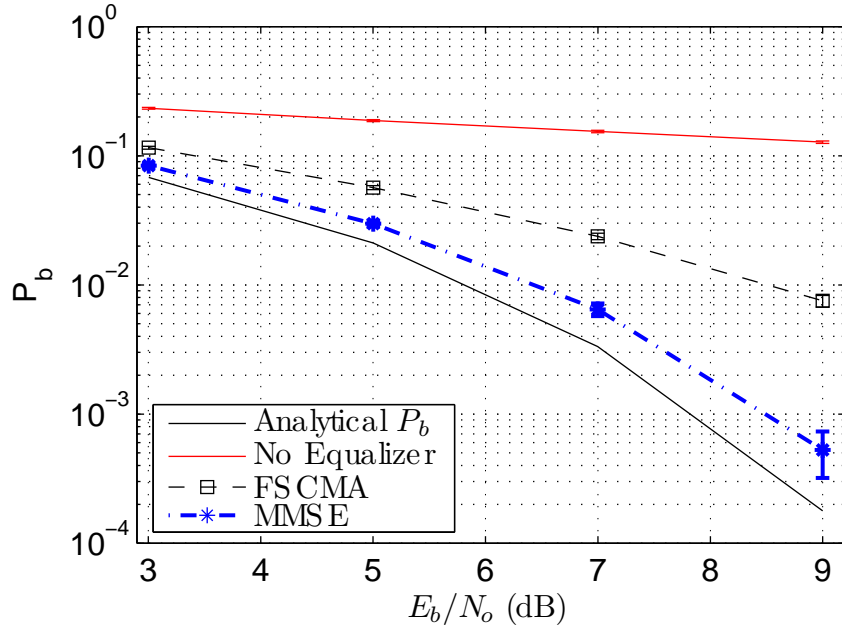
36

Figure 3.8:   Validation with $0.6T_{sym}$ max delay and SRRC β=0.25
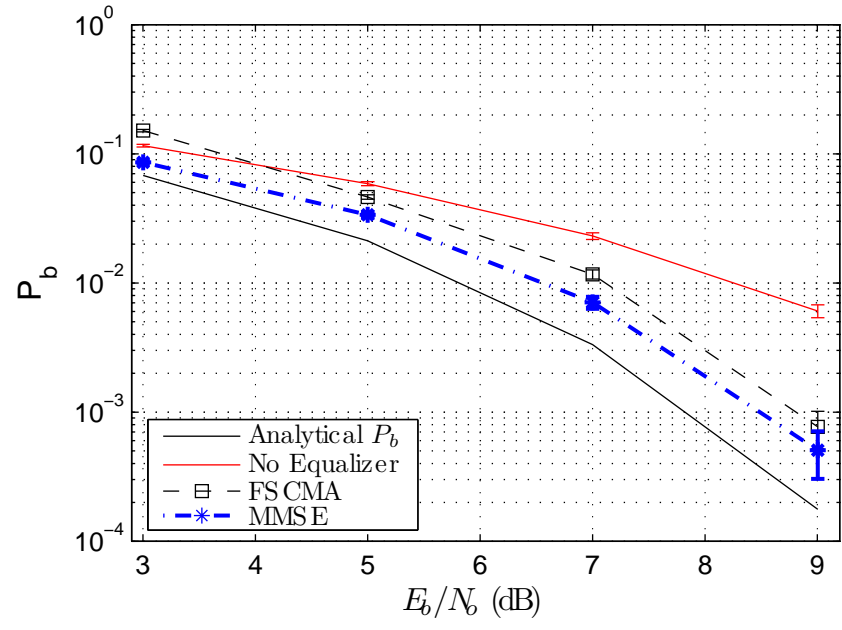

Figure 3.9:   Validation with two ray multipath and SRRC β=0.25

Figure 3.9 and Figure 3.10 show the simulation performance for the 2 and 4 ray multipath models in the absence of symbol dither, respectively. The bit error rate performance of both the CMA and cooperative MMSE equalizers is in the region

37

between the symbol spaced receiver performance and the analytical binary DPSK performance curve, indicating that both equalizers are partially equalizing the multipath interference present. The CMA algorithm uses an adaptive update strategy presented in Section 2.4.3, and as such has a certain amount of variation in the equalizer filter taps derived from the step size, μ. This could be a contributing factor to the degraded P_b performance relative to the cooperative MMSE equalizer structure.
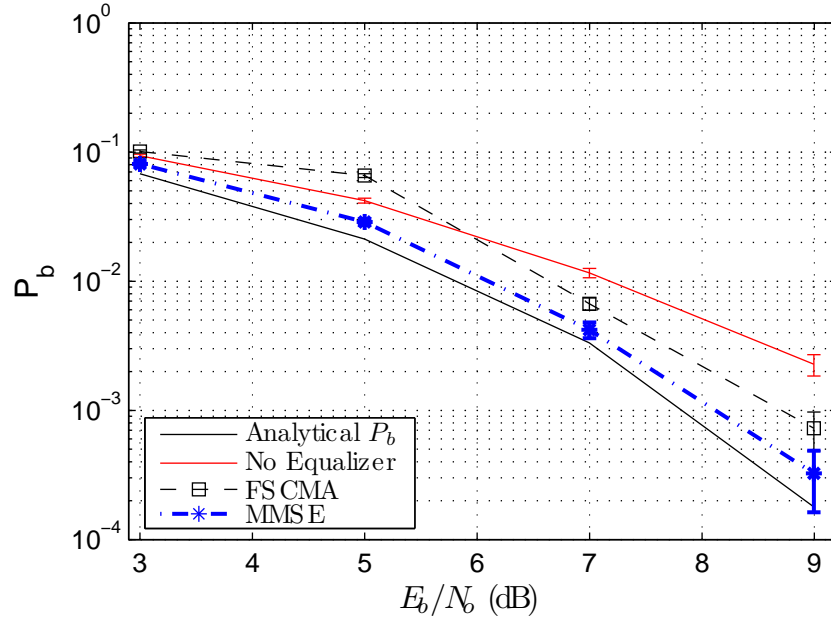

Figure 3.10:   Validation with four ray multipath and SRRC β=0.25

Figure 3.11 and Figure 3.12 show the validation results for the 2 and 4 ray models with symbol timing dither effects included. In both of these figures the cooperative MMSE equalizer structure performs better than its non-cooperative CMA counterpart, providing a performance improvement of approximately 4 dB in terms of bit error rate at $P_b = 4 \times 10^{-2}$. However, the MSE equalizer performance also suffers statistically significant degradation from the analytical P_b curve. These validation results are consistent with prior results presented in [8], and indicate that the various parts of the simulation model are functioning correctly. The effects on bit error rate for a full range of random multipath channels, max symbol timing delays, and pulse shapes is presented in Chapter IV.
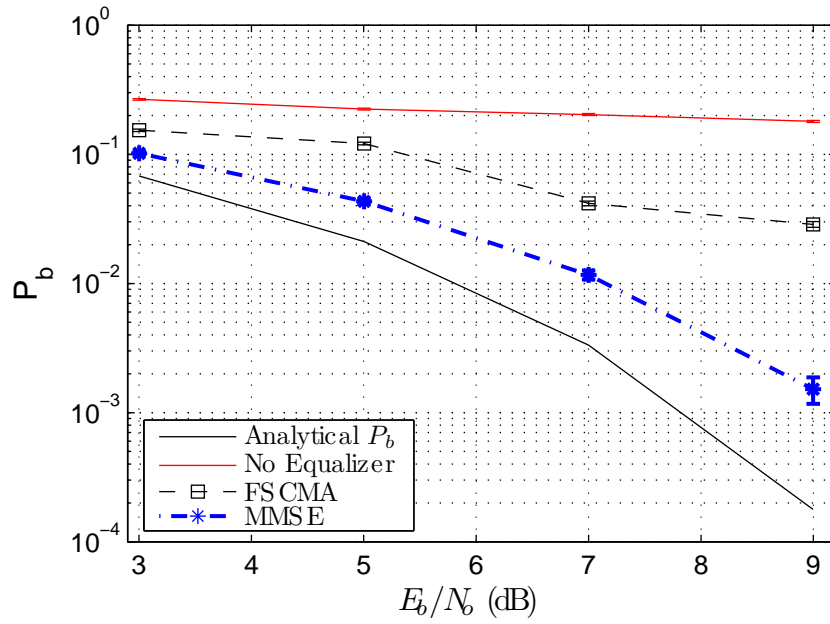
38

Figure 3.11:   Validation with two ray multipath, $0.6T_{sym}$ max delay and SRRC β=0.25
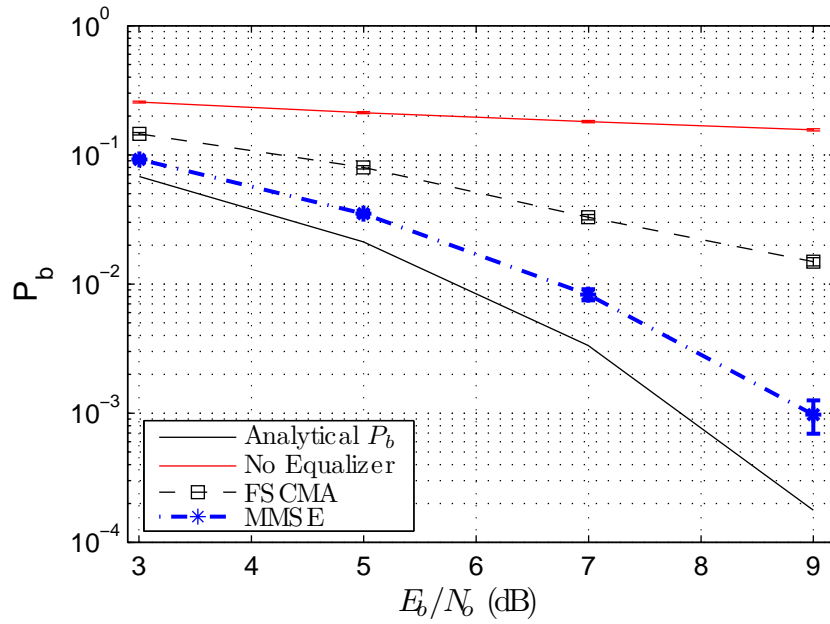

Figure 3.12:   Validation with four ray multipath, $0.6T_{sym}$ max delay and SRRC β=0.25

3.6.2 Simulation Parameters.   This section provides two tables summarizing the simulation parameters used in this thesis for the reader's convienience. Table 3.2 provides a list of all of the global simulation parameters, while Table 3.3 details the parameters used by both the cooperative and non-cooperative receiver structures used in simulation.

Table 3.2:   Simulation Parameters

P	Number of samples per symbol period
M	Number of symbols in the DPSK constellation
Pulse Shape	Pulse shape in the transmitter and the corresponding matched filter
$\mathbf{d}$	Delay code sequence used to determine the delay of each transmitted symbol
p_{max}	Maximum allowable delay in the sequence $\mathbf{d}$
$\mathbf{h}_{phys}$	Physical channel model
SNR	Signal-to-noise ratio as measured the receiver input
O	Number of samples per symbol period after receiver downsampling

Table 3.3: Equalization Parameters

Baseline	N/A	No parameters necessary
FS CMA	μ	Gradient descent step size
	M	Number of taps in the equalizer (equalizer length)
	N	Number of symbols used to train the equalizer
Modified MMSE	δ	Impulse response delay to which the equalizer converges (in symbol periods)
	$\hat{L}$	Estimate of the length of the effective channel (in symbol periods)

41

IV. Results and Analysis

4.1 Overview

This chapter presents performance results of a symbol timing dither system under multipath conditions. Section 4.2 presents a performance comparison of differing β valued SRRC pulse shapes to determine what effect the severity of the pulse shape roll off has on bit error performance. Section 4.4 presents results of a two ray multipath model under a variety of symbol dither conditions, and Section 4.5 examines the performance of a four ray multipath model. Both models are constructed according to the parameters provided in Section 3.4.1.

Results in this chapter were generated using N=1000 randomly generated symbols for both training of the non-cooperative CMA receiver and a unique random set of 1000 symbols for symbol estimation, with N symbols being transmitted over each of the random channels. The BER results are then averaged together to provide a robust picture of system performance under the tested conditions. The confidence intervals shown in figures within Sections 4.4 and 4.5 correspond to 95% confidence intervals based on (4.1) derived from [7]

$$\pm Z_{\frac{\alpha}{2}} \frac{\sigma}{\sqrt{n}} \tag{4.1}$$

where $Z_{\frac{\alpha}{2}}$ corresponds to 1.96 for a 95% confidence, n is the number of samples (in this case the number of randomly generated channels), and σ is the standard deviation of the calculated P_b data. The standard deviation is calculated by taking the BER of each channel and then taking the standard deviation of the resulting vector. The results presented in Section 4.4 and Section 4.5 are separated between well-behaved channel performance plots and poorly performing channel plots. The process used to define a channel as well-behaved or poorly performing is presented in Section 4.3, and results in 35 well-behaved channels and 15 poor performance channels for the two ray multipath model and 44 well-behaved, 6 poorly performing channels for the four ray multipath model. Table 4.1 provides an overview of the results presented.

42

Table 4.1:   Table of experiments

Figure	β	Max Dither (T_{sym})	E_b/N_o	Multipath Model
4.1	0	full range	9 dB	none
4.2	0.25	full range	9 dB	none
4.3	0.5	full range	9 dB	none
4.8	0.5	0.6	3-15 dB	random 2 ray
4.9	0.5	0.99	3-15 dB	random 2 ray
4.10	0.5	full range	9 dB	random 2 ray
4.11	0.5	0.6	3-9 dB	bad random 2 ray
4.12	0.5	0.99	3-15 dB	random 4 ray
4.13	0.5	0.6	3-15 dB	random 4 ray
4.14	0.5	full range	9 dB	random 4 ray
4.15	0.5	0	3-9 dB	bad random 4 ray
4.16	0.5	0.6	3-9 dB	bad random 4 ray
4.17	0.5	0	9 dB	bad random 4 ray

4.2   Pulse Shape Performance

This section examines the effects of varying the roll off factor β of the SRRC pulse shape used throughout this thesis. Figure 4.1, Figure 4.2, and Figure 4.3 show the P_b achieved by each equalizer structure as the timing symbol dither range is varied in the absence of any multipath interference. All plots shown are held constant at E_b/N_o of 9 dB for comparison. As the β value increases from 0 to 0.5, the pulse shape contains less energy outside the main lobe of the pulse, resulting in less ISI as the symbol dither increases. Also, for β=0.5, the cooperative MSE equalizer structure suffers no significant degradation in terms of bit error performance until the symbol dither range exceeds $0.6T_{sym}$. This is a marked increase from the β=0 case, where the MSE equalizer begins to degrade at a symbol dither range of $0.2T_{sym}$. The results for β=0.25 fall somewhere between the performance of β=0 and β=0.5, offering an intermediate step that generates less ISI than the β=0 case.
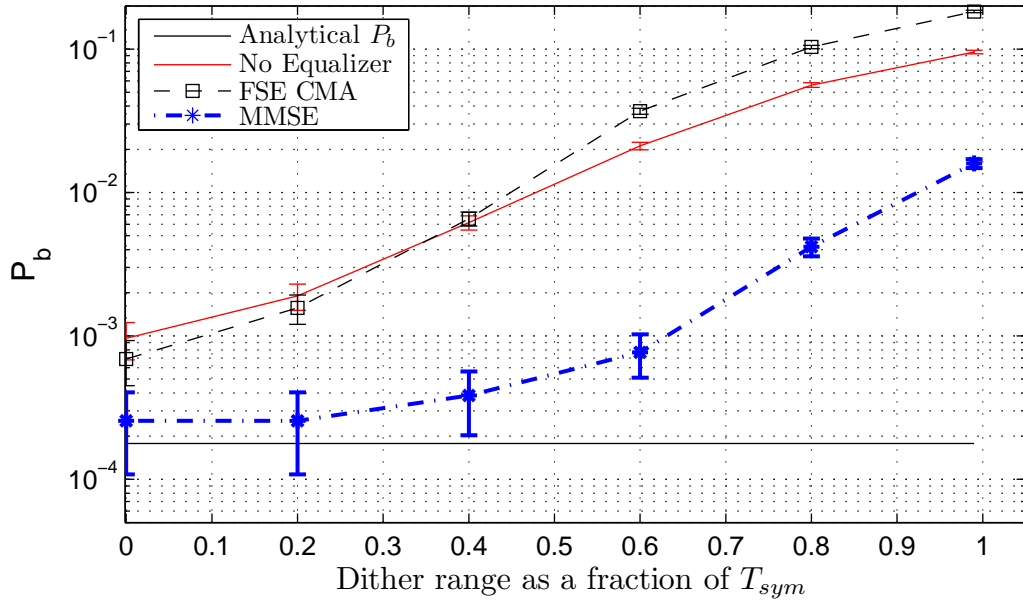
43

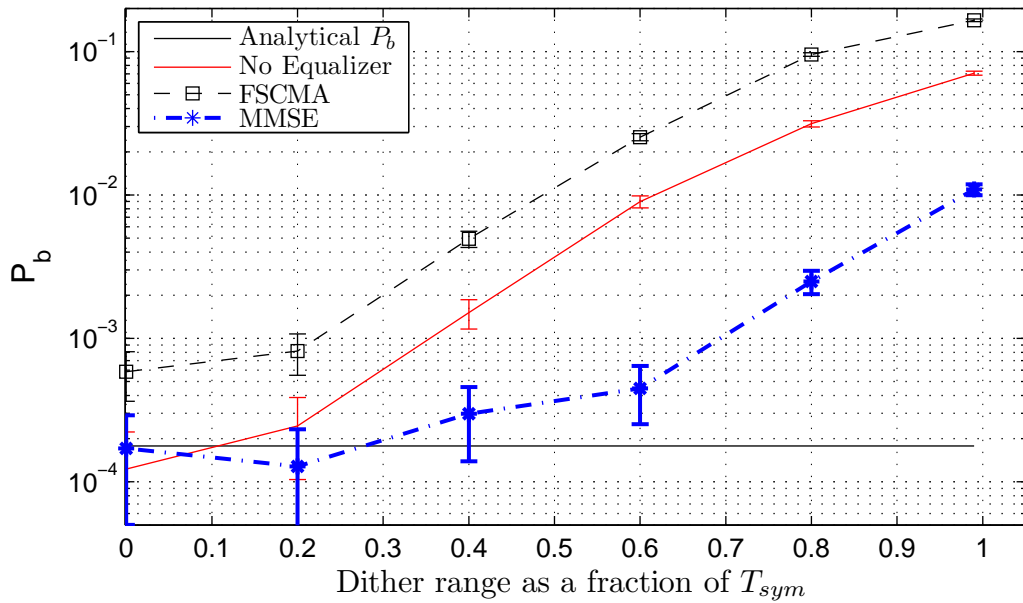Figure 4.1:   Bit Error Comparison for SRRC $\beta=0$ at $E_b/N_o = 9$ dB

Figure 4.2:   Bit Error Comparison for SRRC $\beta=0.25$ at $E_b/N_o = 9$ dB

For no symbol timing dither, all three pulse shapes and equalizers result in P_b = 10^{-3} or better, and are close to the analytical curve, as is expected from validation exercises shown in Chapter III. As β increases, there is a small improvement across all equalizer structures as the symbol timing dither range increases; 10-20% of an
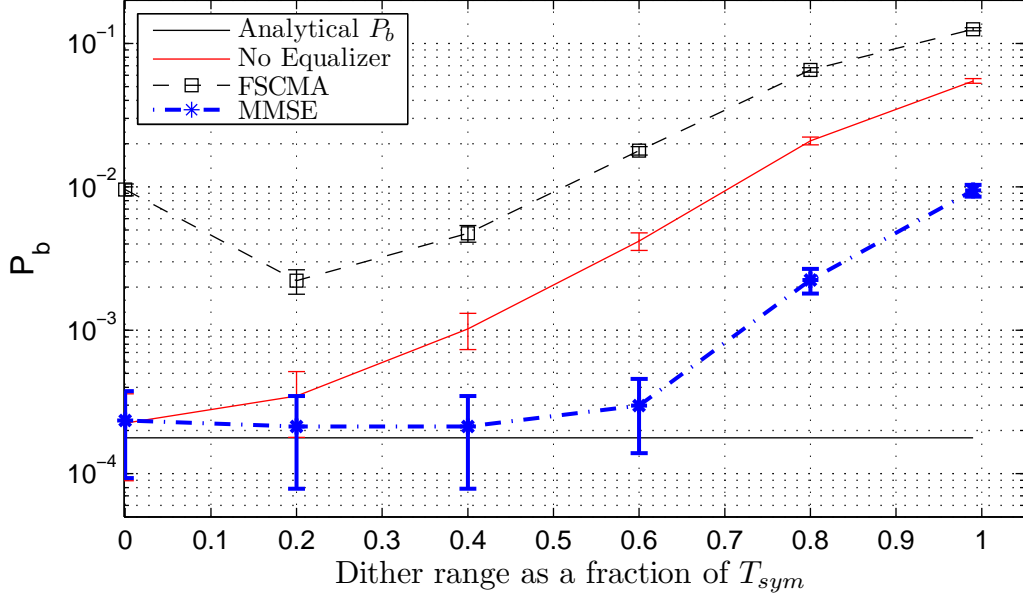
Figure 4.3:   Bit Error Comparison for SRRC β=0.5 at $E_b/N_o = 9$ dB

order of magnitude. As β=0.5 gives slightly better bit error performance across all equalizer structures, all other results presented in this chapter utilize this pulse shape.

4.3 Multipath Channel Validation

To validate each randomly generated multipath channel, the BER was recorded over 5000 transmitted symbols. These bit error rates were then used to sort the channels from best to worst in terms of P_b performance. For both the two ray and four ray groups of multipath channels, an order of magnitude breakpoint existed in channel performance. Channel models that provided equalization results better than this threshold are defined as well-behaved, and those that generated BERs in excess of this threshold are defined as poorly performing. Examples of these randomly generated multipath channels are shown in Figure 4.4 and Figure 4.5.

Figure 4.6 shows the results of applying the determined MSE equalization filter to a well-behaved four ray multipath channel with no timing symbol dither. The large centered impulse demonstrates that a majority of the multipath effects have been removed by the equalization process. Figure 4.7 shows the results of this process
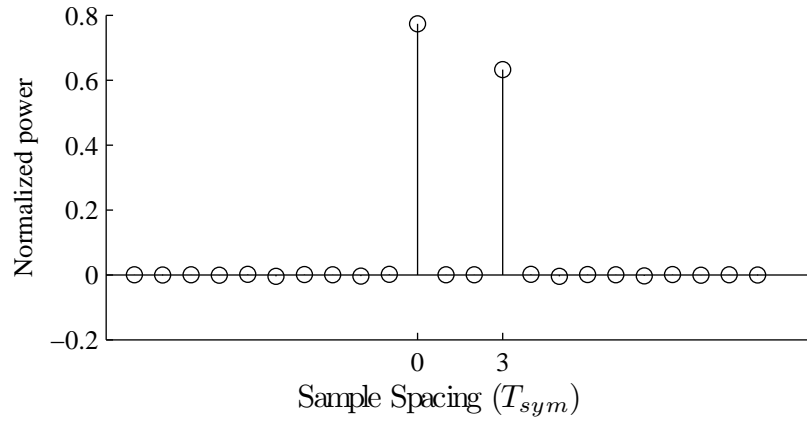
45

Figure 4.4:   Poor Performance Two Ray Multipath Model Normalized channel before equalization at $E_b/N_o = 9$ dB
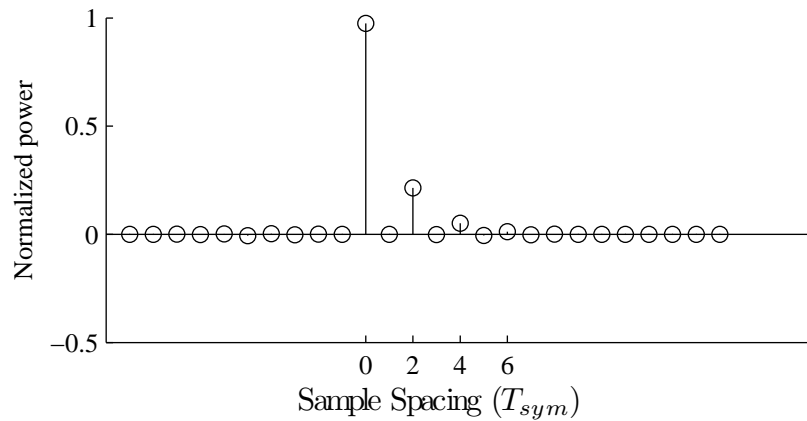

Figure 4.5:   Good Performance Four Ray Multipath Model Normalized channel before equalization at $E_b/N_o = 9$ dB

for a poorly performing two ray multipath model with no timing symbol dither. The lack of a large impulse relative to the others indicates poor equalization performance.
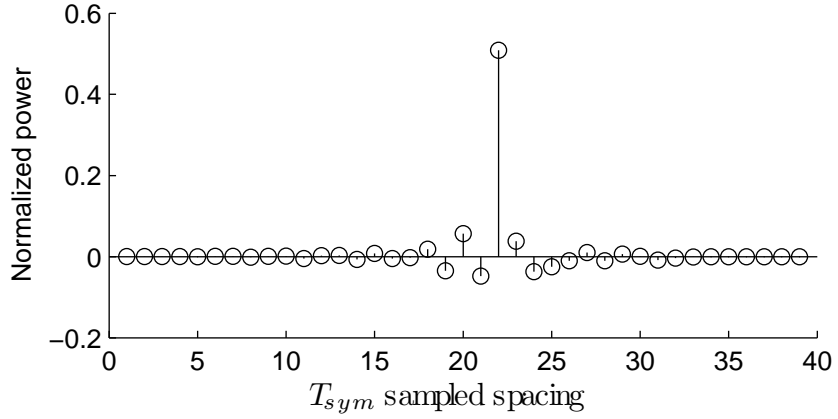
46

Figure 4.6:   Good Performance Four Ray Multipath Model Normalized channel after equalization at $E_b/N_o = 9$ dB
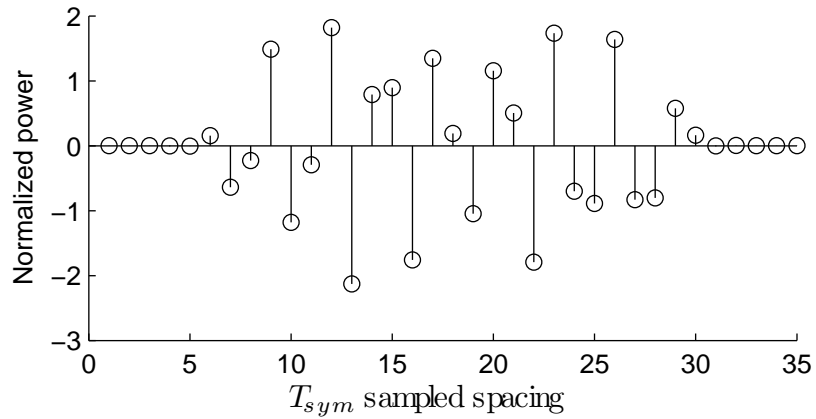

Figure 4.7:   Poor Performance Two Ray Multipath Model Normalized channel after equalization at $E_b/N_o = 9$ dB

Inspection of the coefficients of the poorly performing channels in terms of P_b for both the 2 ray and 4 ray models revealed that each contained a multipath reflection of near equal normalized power as the line of sight path. In order to understand this behavior, the z transform of a poorly performing channel is examined. The z transform is given in (4.2) [11].

$$X(z) = \sum_{-\infty}^{\infty} x[n]z^{-n} \tag{4.2}$$

47

The two ray channel model for a poor performance channel can be approximated as $h = [1\ 1]$. Taking the z transform of h yields the result shown in (4.3).

$$H(z) = 1 + z^{-1} = \frac{(z+1)}{z} \qquad (4.3)$$

This results in a zero on the unit circle, and as the equalizer attempts to invert the channel effects to remove them, this zero will become a pole after inversion. This pole on the unit circle means that the channel approximated by h above does not invert well, and prevents proper calculation of equalization filter coefficients. These poorly inverting channels dominate the P_b performance when all 50 random channels are averaged together, so the poor performance channels are separated out and presented separately from the well-behaved channel performance when presented in Chapter IV.

4.4   *Two Ray Model Multipath Performance*

The results presented in this section are divided into two parts, with the performance over well-behaved two ray random multipath models presented first, followed by results achieved using poorly behaved two ray models presented in Section 4.4.1. Figure 4.8 and Figure 4.9 present the results achieved using the randomly generated well-behaved two ray multipath channels. For a symbol timing dither range of $0.6T_{sym}$, the MSE cooperative receiver achieves a BER of $P_b = 2 \times 10^{-2}$ with approximately 7 dB less E_b/N_o. Through $E_b/N_o = 15$ dB, both non-cooperative receiver structures BERs remain in excess of 10^{-2}. The BER performance of the MSE cooperative receiver asymptotically approaches $P_b = 5 \times 10^{-3}$ at $E_b/N_o = 11$ dB, and remains stable for higher values of E_b/N_o. Due to the power in the multipath model being normalized, increasing the signal power also increases the power of the multipath reflection, creating a BER breakpoint for the MSE equalizer structure used in these simulations. Figure 4.9 also shows this asymptotic behavior in the MSE equalizer performance, but the BER achieved at E_b/N_o has yet to surpass the breakpoint value of 5×10^{-3} noted in Figure 4.8. For the full range of symbol dither presented here, neither of
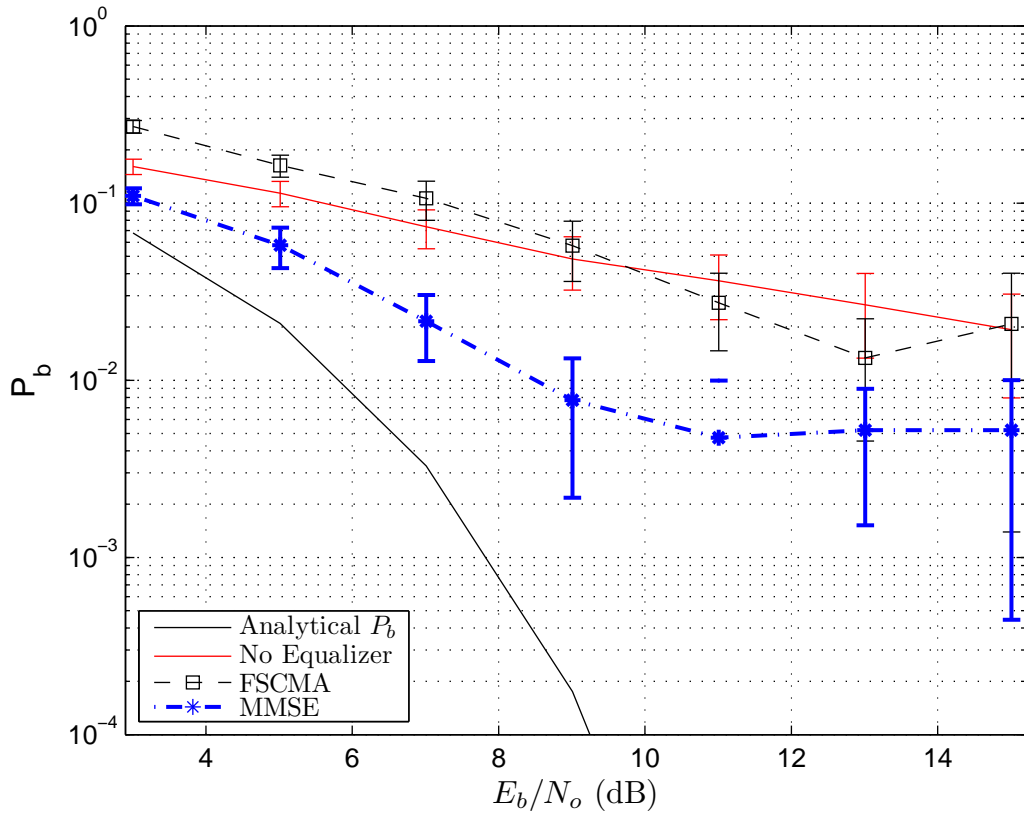
48

Figure 4.8:   Two Ray Random Multipath, Good Channels, $0.6T_{sym}$ Max Delay

the non-cooperative equalizers achieve BERs lower than approximately 0.1, while the MSE equalizer achieves P_b values an order of magnitude better ($P_b = 10^{-2}$). Figure 4.10 shows statistically significant performance improvement of the cooperative MSE equalizer over the non-cooperative equalizers explored in this thesis over the full range of possible symbol timing dither values.
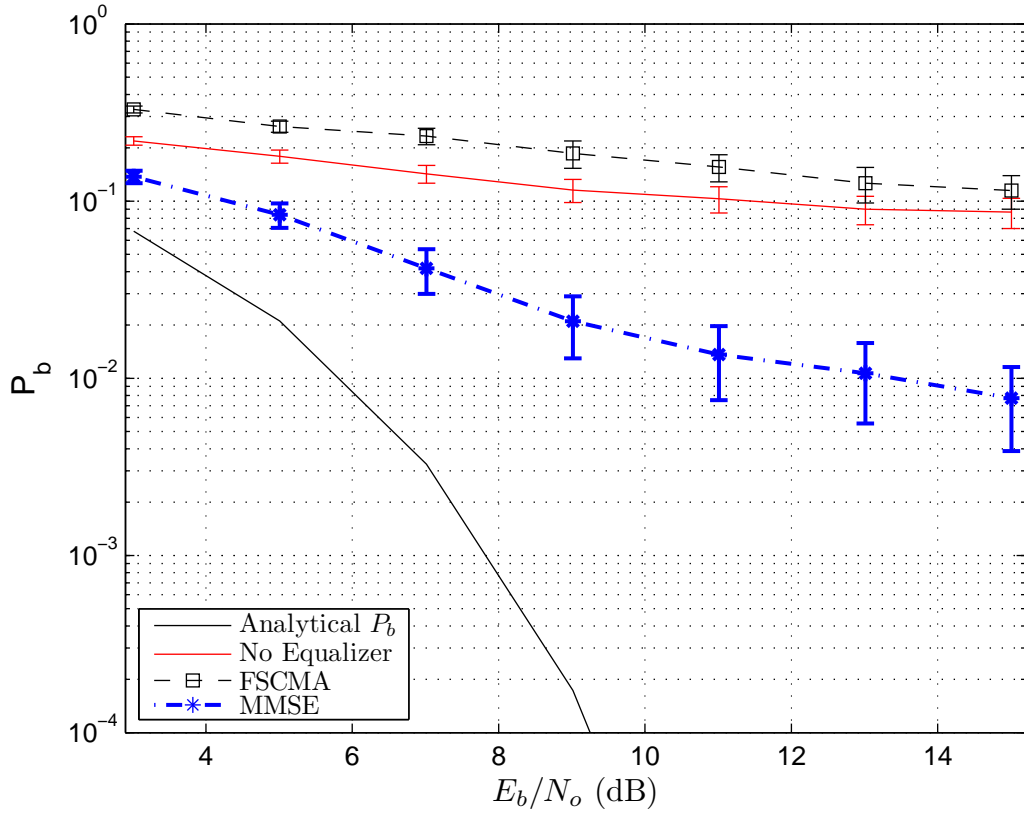
49

Figure 4.9:   Two Ray Random Multipath, Good Channels, $0.99T_{sym}$ Max Delay

4.4.1 Poorly Performing Two Ray Model Performance.   Figure 4.11 shows the performance achieved using the 15 poorly behaved random two ray multipath channels. The difficulty in inverting the channel for equalization discussed in Section 3.4.1 results in the multipath dominating bit error performance, with all equalizer structures generating BERs in excess of $P_b = 10^{-1}$ for a moderate symbol timing dither range value of $0.6T_{sym}$. This behavior indicates that a system using the dither algorithm method equalizer techniques presented is sensitive to the multipath conditions present in the channel at the time of transmission. This is not the fault of the dither algorithm, however, as Figure 4.10 shows a near order of magnitude performance degradation of the CMA equalizer as compared to the MMSE equalizer even for no symbol dither conditions.
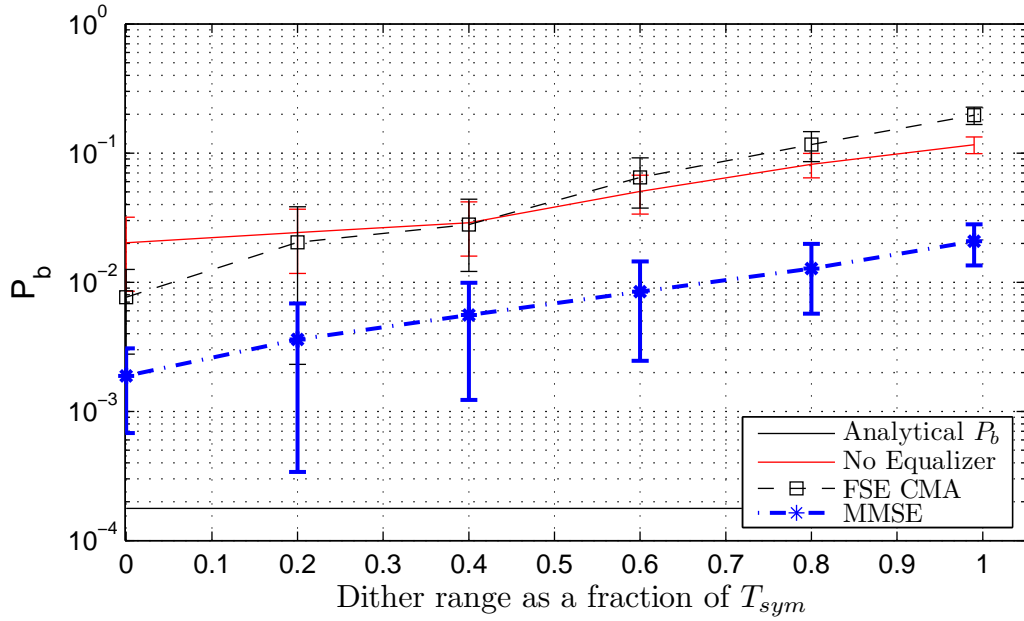
50

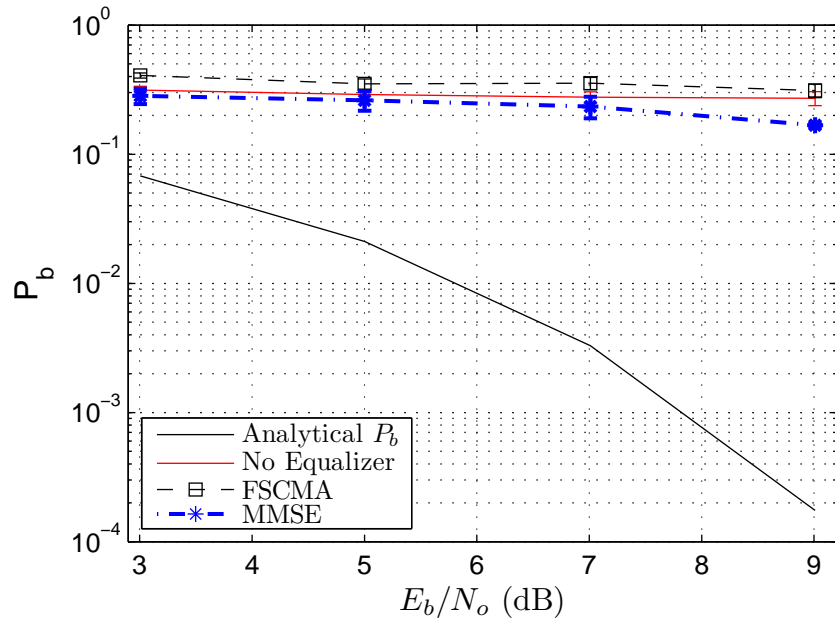Figure 4.10:   Two Ray Random Multipath, Good Channels, $E_b/N_o = 9$ dB

Figure 4.11:   Two Ray Random Multipath, Bad Channels, $0.6T_{sym}$ Max Delay

4.5   Four Ray Model Multipath Performance

Figure 4.12 and Figure 4.13 characterize the BER behavior of the symbol timing dither system in the presence of the 44 random four ray multipath channels. The same

51

asymptotic behavior noted for the two ray multipath models occurs for the four ray multipath as well, occurring at a BER of approximately $P_b = 1 \times 10^{-4}$ for $E_b/N_o = 13$ dB for the MSE equalizer as seen in Figure 4.13. The MSE equalizer provides a BER performance gain of approximately 7 dB relative to explored non-cooperative methods at $P_b = 2 \times 10^{-2}$ and $0.6T_{sym}$ symbol timing dither range. Using the maximum allowable symbol timing dither of $0.99T_{sym}$ (Figure 4.12), the MSE equalizer provides 6 dB of gain over all non-cooperative methods at a BER of 10^{-1}. At $E_b/N_o = 15$ dB, the MSE equalizer outperforms the non-cooperative equalizers by nearly two orders of magnitude, with BERs of 2×10^{-3}. Also, the non-cooperative equalizers produce a BER in excess of 10^{-1} for all E_b/N_o values examined, indicating a theoretical limit for non-cooperative performance under the tested multipath and symbol timing dither conditions. Figure 4.14 shows an approximate order of magnitude BER performance improvement using a cooperative MSE equalizer attuned to symbol timing dither over non-cooperative equalization methods for all possible ranges of symbol timing dither.
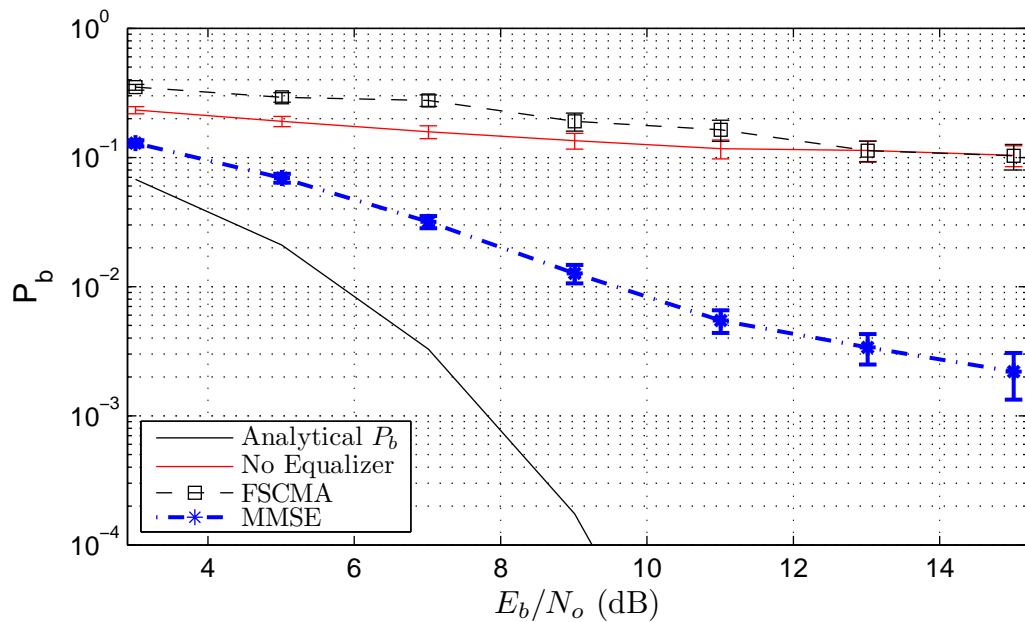

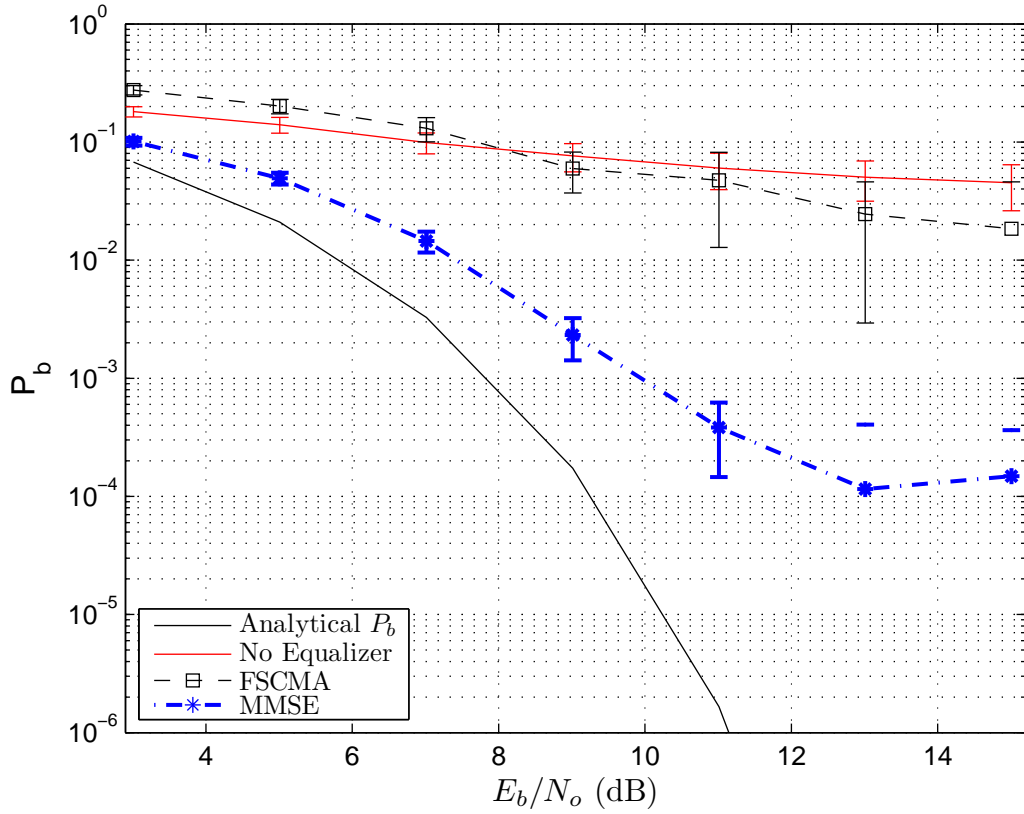Figure 4.12:   Four Ray Random Multipath, Good Channels, $0.99T_{sym}$ Max Delay

52

Figure 4.13:   Four Ray Random Multipath, Good Channels, $0.6T_{sym}$ Max Delay

4.5.1   Poorly Performing Four Ray Model Performance.   Figure 4.15 and Figure 4.16 show the performance achieved using the 6 poorly behaved random four ray multipath channels. The difficulty in inverting the channel for equalization discussed in Section 3.4.1 results in the multipath dominating bit error performance as seen for the poorly performing two ray model channels, with all equalizer structures generating BERs in excess of $P_b = 10^{-1}$ for a both a symbol timing dither range value of 0.4 and $0.6T_{sym}$. This behavior indicates that the dither algorithm method utilizing the equalizer techniques presented is sensitive to the multipath conditions present in the channel at the time of transmission. As in the two ray model results, this is not the fault of the dither algorithm. Figure 4.14 shows a near order of magnitude performance degradation of the CMA equalizer as compared to the MMSE equalizer for no symbol dither conditions. Figure 4.17 repeats the experiments performed in Figure 4.15 and Figure 4.16 with no symbol timing dither, resulting in comparable
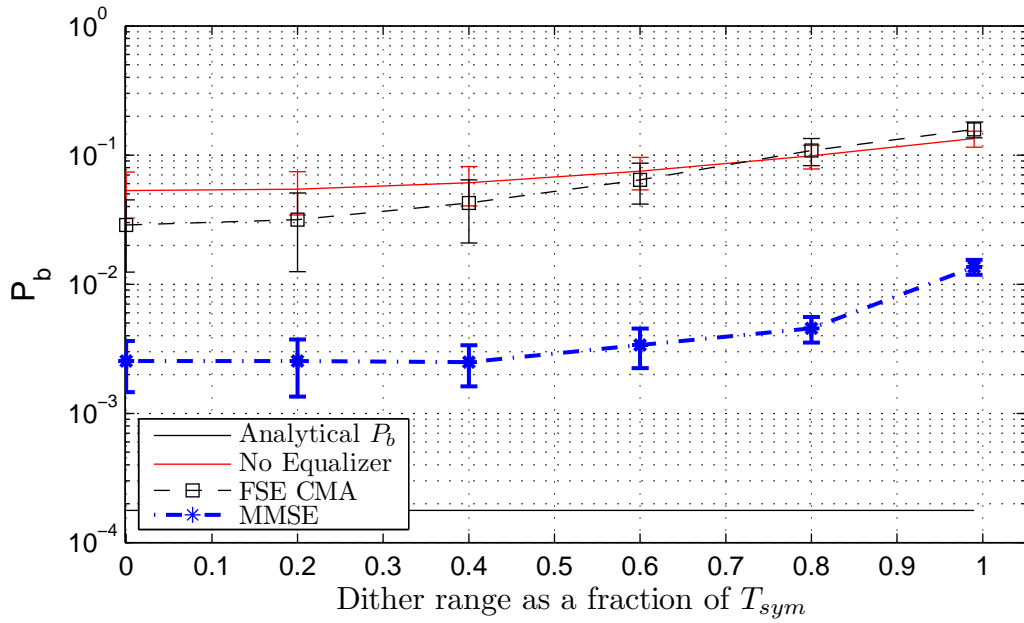
53

Figure 4.14:   Four Ray Random Multipath, Good Channels, E_b/N_o=9 dB

bit error performance for all equalization schemes. This indicates that the sensitivity of the symbol timing dither system to multipath conditions noted above is due to the difficulty involved in equalizing certain multipath channels, not any internal flaw with the dither scheme.
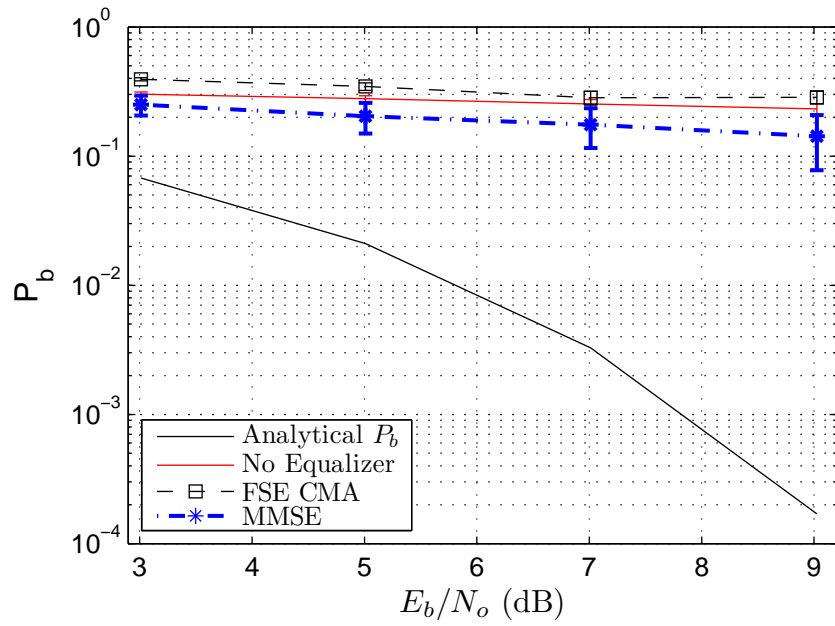
54

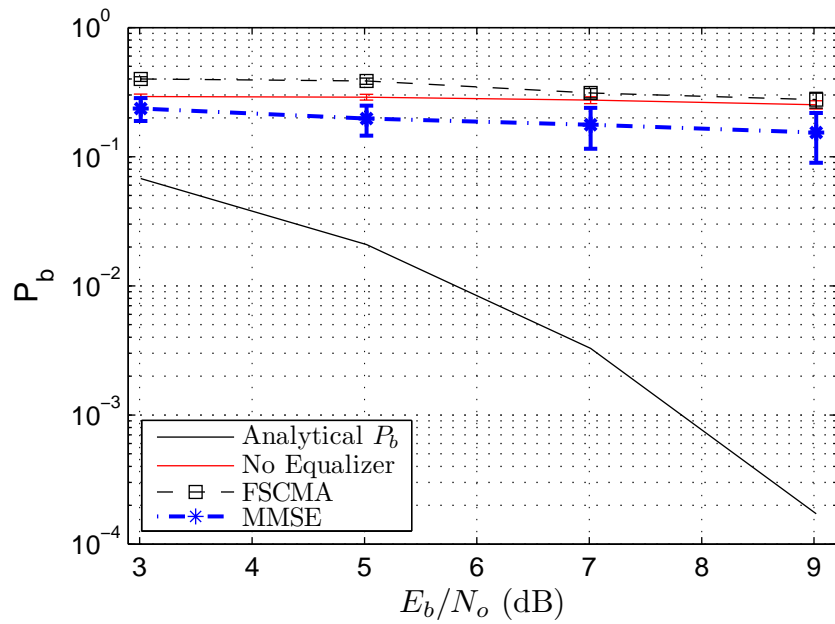Figure 4.15:   Four Ray Random Multipath, Bad Channels, $0.4T_{sym}$ Max Delay

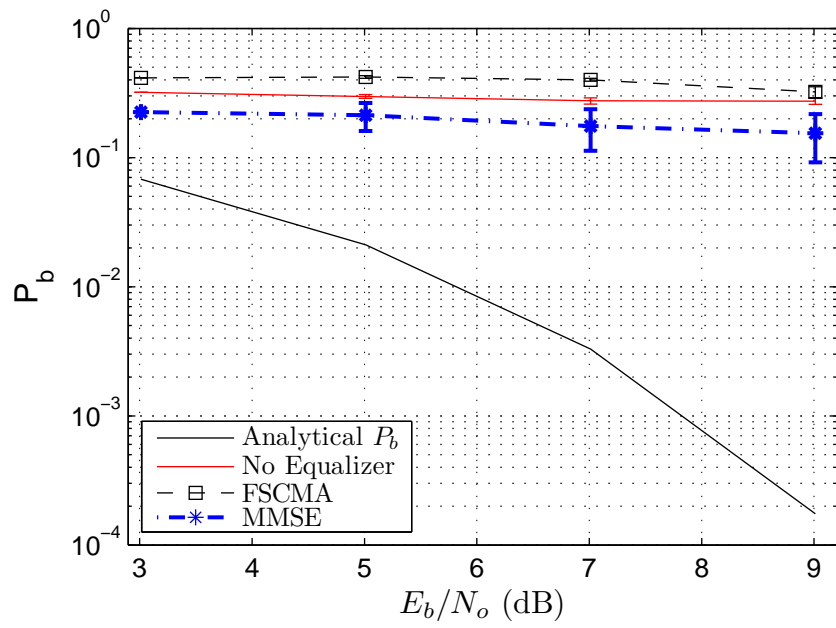Figure 4.16:   Four Ray Random Multipath, Bad Channels, $0.6T_{sym}$ Max Delay

Figure 4.17: Four Ray Random Multipath, Bad Channels, no symbol timing dither

56

V. Conclusions and Recommendations

5.1 Conclusions

This thesis tests the performance of an LPI system implemented using the symbol timing dither in the presence of multipath channel interference [8]. A cooperative receiver structure is shown to provide significant performance improvement over tested non-cooperative receiver structures for a binary DPSK modulated waveform. The timing dither coupled with multipath interference creates ISI that is not explicitly accounted for in non-cooperative receiver designs, with the maximum allowed symbol timing dither range and pulse shape used determining the severity of the induced ISI for a particular multipath interference channel.

For both the two and four ray randomly generated multipath channel models, a cooperative MMSE equalizer structure having knowledge of and synchronization with the transmitted symbol timing dither can be used to achieve a factor of 10 BER performance gain over non-cooperative equalizer methods. Typical gains of the MSE equalizer over tested non-cooperative equalization techniques of 6-8 dB were achieved at BERs of $P_b = 10^{-1}$. When using the maximum allowable range of symbol timing dither, $0.99T_{sym}$, non-cooperative equalization techniques consistently produced BERs in excess of 10^{-1} even for large values of E_b/N_o. The MSE equalizer performance also exhibited an upper limit, asymptotically approaching BERs of $P_b = 5 \times 10^{-3}$ and 1×10^{-4} for the two and four ray multipath models, respectively. The MMSE equalizer structure used in this thesis is computationally expensive, requiring a matrix inverse operation for each transmitted symbol. Also, for certain randomly generated multipath channels, this inversion operation was not well-behaved, and resulted in poor equalization results for all equalizers. This is not necessarily due to equalizer or system issues, as some channels are simply difficult to equalize effectively. This indicates a certain amount of sensitivity to the multipath channel conditions on the part of a symbol timing dither system. Under well-behaved and invertible multipath interference conditions, effective symbol recovery of a transmitted LPI waveform

making use of symbol timing dither is feasible assuming a cooperative receiver with knowledge of the dither pattern.

5.2   Recommendations for Further Study

Several areas for further study related to this thesis are summarized in this section.

It is possible to alter the design of the symbol timing dither algorithm. The algorithm used for this thesis always followed a uniform probability density function, but many other distributions could be used. Also, the results here are limited to binary DPSK modulation. Other modulation techniques could be investigated for use with an LPI system based on symbol timing dither.

A limited set of possible multipath models were used in this thesis to characterize a symbol timing dither waveform's performance in multipath interference. These models used fixed time delays to ensure that all the channels used were linear time invariant. Further research could characterize the symbol timing dither waveform's performance under time varying multipath conditions.

Additional cooperative and non-cooperative receiver designs could be examined for use with symbol timing dither. A small subset of the possible receiver designs were tested in this thesis, and these could be improved upon or new receiver structures and equalization techniques could be examined.

Bibliography

1. A, Shaw, M. Jamali, and N. Wilkins. "Toward Bandwidth Invariance of Spatial Processing in the Non-Cooperative Receiver". *Fourth IEEE Workshop on Sensor Array and Multichannel Processing, 2006.*, 556–560. 2006.

2. Bucher, M. L. "Simulation of Multipath Fading/Ghosting For Analog and Digital Television Transmission in Broadcast Channels". *IEEE Transactions on Broadcasting*, 38(4):256–262, December 1992.

3. Burr, A. G. "The Multipath Problem: An Overview". *Proceedings of the IEE*, July-August 1996.

4. Ding, Z., R. A. Kennedy, B. D. O. Anderson, and C. R. Johnson Jr. "Ill-convergence of Godard blind equalizers in data communication systems". *IEEE Transactions on Communications*, 39(9):1313–1327, September 1991.

5. Haykin, S. *Adaptive Filter Theory*. Prentice Hall, Upper Saddle River, New Jersey, 2002.

6. Johnson, Jr., C. R., P. Schniter, T. J. Endres, J. D. Behm, D. R. Brown, and R. A. Casas. "Blind equalization using the constant modulus criterion: a review". *Proceedings of the IEEE*, 86(10):1927–1950, October 1998.

7. Leon-Garcia, A. *Probability and Random Processes for Electrical Engineering*. Addison Wesley Longman, Reading, Massachusetts, 1994.

8. Liefer, N. *Signal Processing Design of Low Probability of Intercept Waveforms via Intersymbol Dither*. Master's of Science, Air Force Institute of Technology, 2950 Hobson Way, WPAFB, OH 45433-7765, March 2008.

9. McLendon, J. W. *Information Warfare: Impacts and Concerns*, 171–200. Battlefield of the Future: 21st Century Warfare Issues. University Press of the Pacific, Maxwell AFB, 1998.

10. Moulines, E., P. Duhamel, J. F. Cardoso, and S. Mayrargue. "Subspace methods for the blind identification of multichannel FIR filters". *IEEE Transactions on Signal Processing*, 43(2):516–525, February 1995.

11. Oppenheim, A., R. Schafer, and J. Buck. *Discrete-Time Signal Processing*. Prentice Hall, Upper Saddle River, New Jersey, 1999.

12. Poor, H. V. *An Introduction to Signal Detection and Estimation*. Dowden & Culver, USA, 1994.

13. Proakis, J. G. *Digital Communications*. McGraw-Hill, Boston, 1995.

14. Sklar, B. *Digital Communications: Fundamentals and Applications*. Prentice Hall, Upper Saddle River, New Jersey, 2001.

15. Stoney, P. R. "Modern Communications: A Wise Investment". *Air University Review*, July-August 1973.

16. Tong, L., G. Xu, and T. Kailath. "Blind identification and equalization based on second-order statistics: a time domain approach". *IEEE Transactions on Information Theory*, 40(2):340–349, March 1994.

17. Torrieri, D. J. *Principles of Secure Communication Systems.* Artech House, Boston, 1992.

18. Xue, Y. and X. Zhu. "Wireless channel tracking based on self-tuning second-order LMS algorithm". *IEE Proceedings: Communications*, 150(2):115–120, April 2003.

Vita

Jonathan Keen was born in Richlands, VA in 1980. After graduating from Richlands High School in Richlands, VA in 1998, he attended the University of Tennessee Knoxville on an ROTC scholarship. He graduated with honors, earning a Bachelor of Science Degree in Electrical Engineering in 2003 and was commissioned as a second lieutenant in the United States Air Force. Prior to Attending the Air Force Institute of Technology, Jonathan was an orbital analyst and a crew commander for the Defense Satellite Communications System (DSCS III) communications satellite constellation while serving in the 3rd Space Operations Squadron, Schriever AFB, CO. Upon graduation, Capt Keen will be assigned to the National Reconnaissance Organization in Chantilly, VA.

REPORT DOCUMENTATION PAGE

1. REPORT DATE *(DD–MM–YYYY)*	2. REPORT TYPE	3. DATES COVERED *(From — To)*
26–03–2009	Master's Thesis	Sept 2007 — Mar 2009

4. TITLE AND SUBTITLE

Low Probability of Intercept Waveforms
via Intersymbol Dither
Performance Under Multipath Conditions

5a. CONTRACT NUMBER

5b. GRANT NUMBER

5c. PROGRAM ELEMENT NUMBER

6. AUTHOR(S)

Jonathan K. Keen, Capt, USAF

5d. PROJECT NUMBER

09ENG243

5e. TASK NUMBER

5f. WORK UNIT NUMBER

7. PERFORMING ORGANIZATION NAME(S) AND ADDRESS(ES)

Air Force Institute of Technology
Graduate School of Engineering and Management (AFIT/EN)
2950 Hobson Way
WPAFB OH 45433-7765

8. PERFORMING ORGANIZATION REPORT NUMBER

AFIT/GE/ENG/09-23

9. SPONSORING / MONITORING AGENCY NAME(S) AND ADDRESS(ES)

Air Force Research Laboratory, Sensors Directorate (Vasu Chakravarthy)
2241 Avionics Circle, Bldg. 620
WPAFB, OH 45433-7131 DSN: 785-6653 X3592
email: Vasu.Chakravarthy@wpafb.af.mil

10. SPONSOR/MONITOR'S ACRONYM(S)

AFRL/RYRE

11. SPONSOR/MONITOR'S REPORT NUMBER(S)

12. DISTRIBUTION / AVAILABILITY STATEMENT

APPROVED FOR PUBLIC RELEASE; DISTRIBUTION UNLIMITED

13. SUPPLEMENTARY NOTES

14. ABSTRACT

This thesis examines the effects of multipath interference on Low Probability of Intercept (LPI) waveforms generated using intersymbol dither. This thesis expands on prior work by examining the effects of multipath interference on cooperative and non-cooperative receiver performance to assess the above method's effectiveness using a more realistic model of the physical transmission channel. The performance of a Minimum Mean Squared Error (MMSE) cooperative equalizer and a Constant Modulus Algorithm (CMA) non-cooperative equalizer are examined. Simulation results suggest that it is possible for cooperative receivers to accurately demodulate a transmitted waveform in multipath conditions, while degrading non-cooperative receiver performance. Several randomly generated multipath channels exhibited extremely poor equalization results, indicating a level of algorithm sensitivity to multipath conditions.

15. SUBJECT TERMS

Secure Communications, Wireless Communications, Signal Processing, Intersymbol Interference, Multipath Transmission, Equalization

16. SECURITY CLASSIFICATION OF:			17. LIMITATION OF ABSTRACT	18. NUMBER OF PAGES	19a. NAME OF RESPONSIBLE PERSON
a. REPORT	b. ABSTRACT	c. THIS PAGE			Richard K. Martin, PhD
U	U	U	UU	77	19b. TELEPHONE NUMBER *(include area code)* (937) 255–3636, x4625 Richard.Martin@afit.edu